

# The clinical KRAS(G12C) inhibitor AMG 510 drives anti-tumour immunity

<https://doi.org/10.1038/s41586-019-1694-1>

Received: 29 March 2019

Accepted: 18 September 2019

Published online: 30 October 2019

Jude Canon<sup>1\*</sup>, Karen Rex<sup>1,17</sup>, Anne Y. Saiki<sup>1,17</sup>, Christopher Mohr<sup>1</sup>, Keegan Cooke<sup>1</sup>, Dhanashri Bagal<sup>2</sup>, Kevin Gaida<sup>1</sup>, Tyler Holt<sup>1</sup>, Charles G. Knutson<sup>3</sup>, Neelima Koppada<sup>3</sup>, Brian A. Lanman<sup>1</sup>, Jonathan Werner<sup>1</sup>, Aaron S. Rapaport<sup>2</sup>, Tisha San Miguel<sup>1</sup>, Roberto Ortiz<sup>3,14</sup>, Tao Osgood<sup>1</sup>, Ji-Rong Sun<sup>1</sup>, Xiaochun Zhu<sup>3,15</sup>, John D. McCarter<sup>1</sup>, Laurie P. Volak<sup>3,16</sup>, Brett E. Houk<sup>4</sup>, Marwan G. Fakih<sup>5</sup>, Bert H. O'Neil<sup>6</sup>, Timothy J. Price<sup>7,8</sup>, Gerald S. Falchook<sup>9</sup>, Jayesh Desai<sup>10</sup>, James Kuo<sup>11</sup>, Ramaswamy Govindan<sup>12</sup>, David S. Hong<sup>13</sup>, Wenjun Ouyang<sup>2</sup>, Haby Henary<sup>4</sup>, Tara Arvedson<sup>2</sup>, Victor J. Cee<sup>1</sup> & J. Russell Lipford<sup>1\*</sup>

*KRAS* is the most frequently mutated oncogene in cancer and encodes a key signalling protein in tumours<sup>1,2</sup>. The KRAS(G12C) mutant has a cysteine residue that has been exploited to design covalent inhibitors that have promising preclinical activity<sup>3–5</sup>. Here we optimized a series of inhibitors, using novel binding interactions to markedly enhance their potency and selectivity. Our efforts have led to the discovery of AMG 510, which is, to our knowledge, the first KRAS(G12C) inhibitor in clinical development. In preclinical analyses, treatment with AMG 510 led to the regression of *KRAS*<sup>G12C</sup> tumours and improved the anti-tumour efficacy of chemotherapy and targeted agents. In immune-competent mice, treatment with AMG 510 resulted in a pro-inflammatory tumour microenvironment and produced durable cures alone as well as in combination with immune-checkpoint inhibitors. Cured mice rejected the growth of isogenic *KRAS*<sup>G12D</sup> tumours, which suggests adaptive immunity against shared antigens. Furthermore, in clinical trials, AMG 510 demonstrated anti-tumour activity in the first dosing cohorts and represents a potentially transformative therapy for patients for whom effective treatments are lacking.

The KRAS oncoprotein is a GTPase and an essential mediator of intracellular signalling pathways that are involved in tumour cell growth and survival<sup>1,2</sup>. In normal cells, KRAS functions as a molecular switch, alternating between inactive GDP-bound and active GTP-bound states<sup>6,7</sup>. Transition between these states is facilitated by guanine nucleotide-exchange factors—which load GTP and activate KRAS—and GTP hydrolysis, which is catalysed by GTPase-activating proteins to inactivate KRAS<sup>2</sup>. GTP binding to KRAS promotes binding of effectors to trigger signal transduction pathways including the RAF–MEK–ERK (MAPK) pathway<sup>8,9</sup>. Somatic, activating mutations in *KRAS* are a hallmark of cancer and prevent the association of GTPase-activating proteins, thus stabilizing effector binding and enhancing KRAS signalling<sup>10</sup>. Although there are clinically approved inhibitors of several MAPK pathway proteins (for example, inhibitors of MEK, BRAF and EGFR) for a subset of tumour types, to date there have been no clinical molecules that are selective for *KRAS*-mutant tumours. Moreover, several MAPK-pathway-targeting therapies are contra-indicated for treatment of *KRAS*-mutant tumours owing to a lack of clinical efficacy<sup>11</sup>. Additionally, non-tumour or non-mutant selective therapies can introduce on-target toxicities due to the inhibition of MAPK signalling in normal cells<sup>12,13</sup>. This might limit the ability to combine such agents with standard-of-care treatments or immunotherapy. Thus, there

is a considerable unmet need for the development of tumour-selective therapies that do not introduce liabilities for normal cells.

*KRAS*<sup>G12C</sup> is present in approximately 13% of lung adenocarcinoma, 3% of colorectal cancer and 2% of other solid tumours<sup>14</sup>. The mutant cysteine of KRAS(G12C) resides adjacent to a pocket (P2) that is present in the inactive GDP-bound form of KRAS<sup>3</sup>. The proximity of P2 and the mutant cysteine led to a broad search for covalent inhibitors, eventually resulting in the identification of ARS-1620<sup>3–5</sup>. This preclinical tool compound was a milestone for proof-of-concept, mutant-selective KRAS inhibition<sup>15</sup>. We identified a series of novel acrylamide-based molecules that utilize a previously unexploited surface groove in KRAS(G12C) to substantially enhance potency and selectivity. Intensive electrophile screening and structure-based design culminated in the discovery of AMG 510, which is, to our knowledge, the first KRAS(G12C) inhibitor to reach clinical testing in humans (clinicaltrials.gov identifier NCT03600883)<sup>16</sup>. Here we present the data on the preclinical activity of AMG 510, its ability to induce tumour-cell killing as monotherapy or when combined with other therapies, and the marked impact of AMG 510 on immune cell infiltration, which renders the tumour microenvironment highly sensitive to immunotherapy. We also present promising evidence for clinical efficacy.

<sup>1</sup>Amgen Research, Amgen Inc, Thousand Oaks, CA, USA. <sup>2</sup>Amgen Research, Amgen Inc, South San Francisco, CA, USA. <sup>3</sup>Amgen Research, Amgen Inc, Cambridge, MA, USA. <sup>4</sup>Amgen Clinical Development, Amgen Inc, Thousand Oaks, CA, USA. <sup>5</sup>City of Hope, Duarte, CA, USA. <sup>6</sup>Indiana University School of Medicine, Indianapolis, IN, USA. <sup>7</sup>The Queen Elizabeth Hospital, Woodville, South Australia, Australia. <sup>8</sup>University of Adelaide, Adelaide, South Australia, Australia. <sup>9</sup>Sarah Cannon Research Institute, Denver, CO, USA. <sup>10</sup>Peter MacCallum Cancer Center, Melbourne, Victoria, Australia. <sup>11</sup>Scientia Clinical Research, Randwick, New South Wales, Australia. <sup>12</sup>Washington University School of Medicine, St Louis, MO, USA. <sup>13</sup>The University of Texas MD Anderson Cancer Center, Houston, TX, USA. <sup>14</sup>Present address: Pfizer, La Jolla, CA, USA. <sup>15</sup>Present address: Takeda, Cambridge, MA, USA. <sup>16</sup>Present address: Celgene, San Diego, CA, USA. <sup>17</sup>These authors contributed equally: Karen Rex, Anne Y. Saiki. \*e-mail: jcanon@amgen.com; jlipford@amgen.com

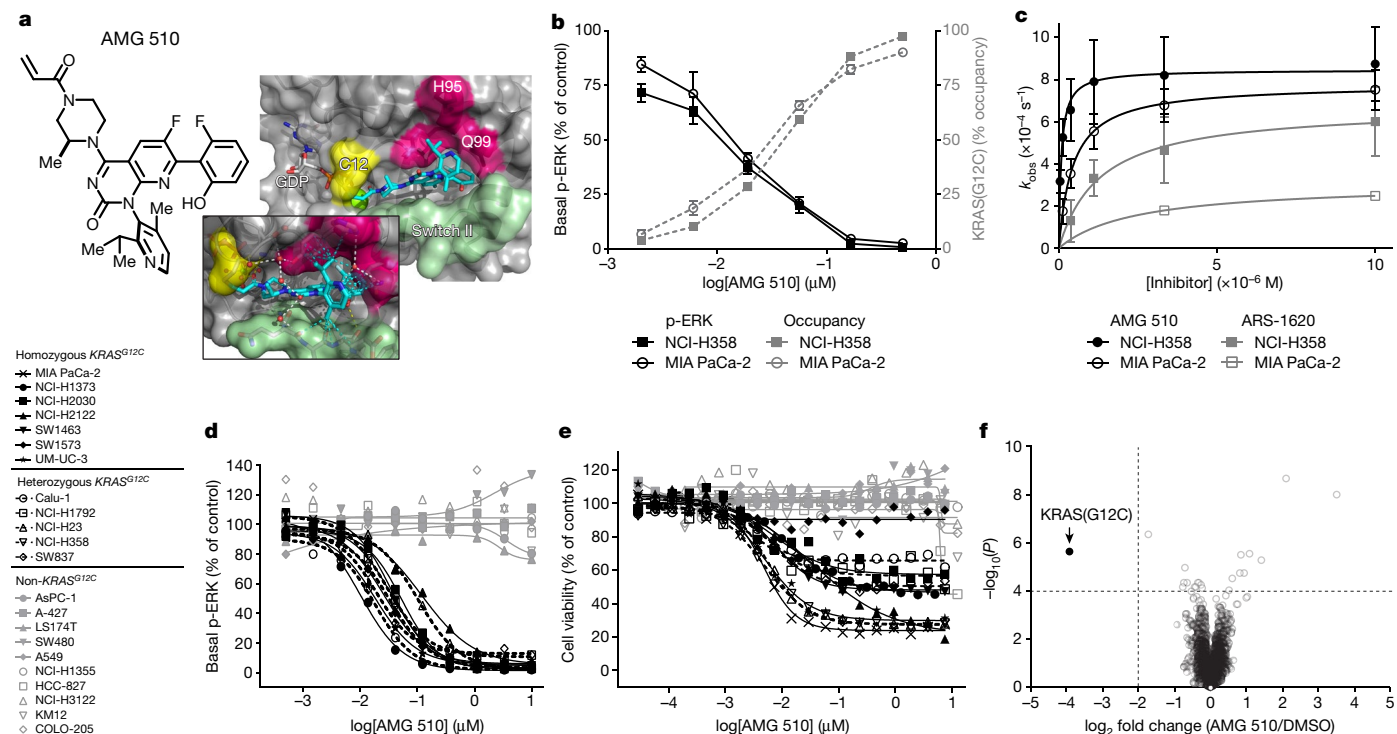


**Fig. 1 | AMG 510 exploits a cryptic groove in KRAS(G12C) to enhance potency and selectivity.** **a**, X-ray co-crystal structure of KRAS(G12C/C51S/C80L/C118S) bound to GDP and AMG 510 at a resolution of 1.65 Å. Cyan dashes, van der Waals contacts; white dashes, water-mediated interactions; yellow dashes, ligand–protein hydrogen bond interactions (PDB: 6OIM). **b**, Inhibition of p-ERK and occupancy of KRAS(G12C) by AMG 510 after a 2-h treatment. Data are mean  $\pm$  s.d.,  $n = 3$  replicates. **c**, Kinetic properties as determined by inhibition of p-ERK.  $k_{\text{obs}}$  and standard error of the curve were determined from nonlinear

curve fitting of experimental values. **d**, **e**, Cellular activity of AMG 510 across a panel of KRAS<sup>G12C</sup> and non-KRAS<sup>G12C</sup> mutant cell lines measured as the inhibition of p-ERK after a 2-h treatment (**d**) and the effects on cell viability after a 72-h treatment (**e**). Representative examples of the data are shown (see Supplementary Table 1 for the number of replicates). **f**, Cysteine proteome analysis of NCI-H358 whole-cell lysates after a 4-h treatment with 1 μM AMG 510 or DMSO.  $n = 5$  independent replicates,  $P$  values were derived from a two-tailed Student's  $t$ -test.

## Enhanced binding and potency of AMG 510

Direct inhibition of KRAS(G12C) was validated by ARS-1620, but the identification of improved inhibitors suitable for clinical testing has proven difficult. One key challenge is suboptimal potency owing to the small volume of the pocket occupied by ARS-1620, which offers limited avenues for additional protein–ligand interactions. This was illustrated by the X-ray crystal structure of the KRAS(G12C)–ARS-1620 covalent complex (Extended Data Fig. 1a), in which hydrogen bonding between ARS-1620 and His95 featured prominently. Our key breakthrough was the discovery that a surface groove, created by an alternative orientation of His95, could be occupied by aromatic rings, which enhanced interactions with the KRAS(G12C) protein<sup>17</sup>. AMG 510 emerged as the top candidate from an optimization campaign of His95 groove-binding molecules, as it represented the convergence of improved potency and favourable development properties. The X-ray co-crystal structure of the covalent AMG 510–KRAS(G12C) complex (Fig. 1a and Extended Data Table 1) highlighted the binding of AMG 510 in the P2 pocket of KRAS. Although portions of the AMG 510 and ARS-1620 ligands are structurally related and overlap (Extended Data Fig. 1b), the His95 groove is a novel feature of the binding of AMG 510 (Fig. 1a and Extended Data Fig. 1b). The highly optimized isopropyl-methylpyridine substituent of AMG 510 that occupied the His95 groove engaged in a continuous network of 25 ligand–protein van der Waals contacts extending from the backbone of helix 2 (His95, Tyr96) to the backbone of the flexible switch II loop (Fig. 1a). These enhanced interactions improved the potency of AMG 510 approximately 10-fold (mean half-maximum inhibitory concentration ( $IC_{50}$ ) = 0.09 μM), as compared to ARS-1620 in a nucleotide-exchange assay with recombinant GDP-bound KRAS(G12C). AMG 510 did not inhibit wild-type KRAS and a non-reactive analogue did not inhibit KRAS(G12C) (Extended Data Fig. 1c, d). The kinetics of the

reaction between AMG 510 and GDP-KRAS(G12C) were measured by mass spectrometry and exhibited a marked improvement compared to ARS-1620 (Extended Data Fig. 1e, f). Relative to cysteine-targeted kinase inhibitors in the clinic<sup>18</sup>, AMG 510 exhibited a larger maximal rate of inactivation ( $k_{\text{inact}}$ ), consistent with the KRAS-induced catalysis mechanism that has previously been described for ARS-1620<sup>15</sup>. The non-specific reactivity of AMG 510 with glutathione was relatively slow ( $t_{1/2} = 196$  min)<sup>19</sup> and within the range of clinical acrylamides<sup>20</sup>.

## AMG 510 inhibits signalling and growth

The cellular activity of AMG 510 was assessed by measuring basal phosphorylation of ERK1/2(p-ERK) and by mass spectrometry to detect the covalent conjugation or occupancy of KRAS(G12C) by AMG 510. In two KRAS<sup>G12C</sup> cell lines, NCI-H358 and MIA PaCa-2, AMG 510 almost completely inhibited p-ERK ( $IC_{50} \approx 0.03$  μM) after a 2-h treatment and was 20-fold more potent than ARS-1620 (Extended Data Fig. 1g). This inhibition closely tracked the occupancy of KRAS(G12C) by AMG 510, with near maximal levels achieved in both assays at around 0.2 μM (Fig. 1b). AMG 510 also potently impaired cellular viability in both NCI-H358 and MIA PaCa-2 ( $IC_{50} \approx 0.006$  μM and 0.009 μM respectively, approximately 40-fold more potent than ARS-1620; Extended Data Fig. 1h). Examining the time and concentration dependence of the inhibition of p-ERK in these lines revealed a kinetic advantage that favoured AMG 510 by approximately 22-fold (Fig. 1c and Extended Data Fig. 1f). The maximal inhibition rate of p-ERK by AMG 510 is approximately twofold greater than the rate-limiting GTP-KRAS(G12C) hydrolysis rate that has recently been proposed<sup>4</sup>. To estimate the GTPase rate by another method, we used a SHP2 inhibitor<sup>21</sup> to eliminate all upstream signalling to KRAS, which yielded a rate ( $9.4 \times 10^{-4}$  s<sup>-1</sup>,  $t_{1/2} = 12.2$  min; Extended Data Fig. 2a) that was congruent with what was observed for AMG 510.

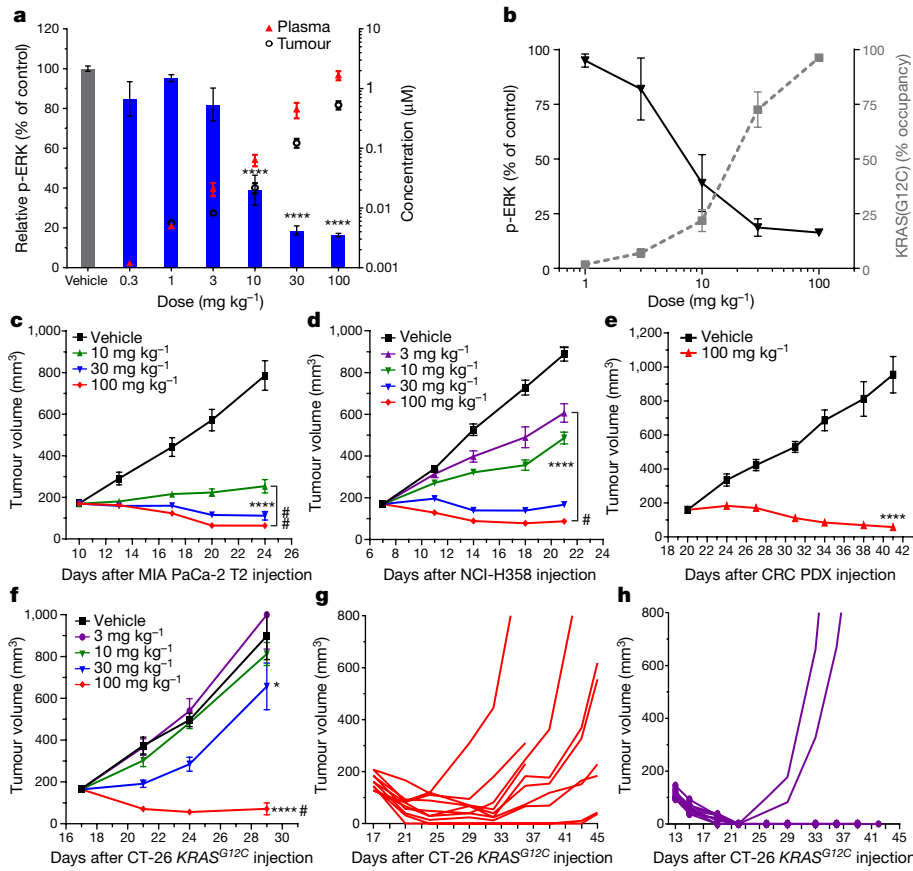


**Fig. 2 | AMG 510 inhibits ERK phosphorylation and growth of KRAS<sup>G12C</sup>-mutant tumours**

**in vivo.** **a**, p-ERK levels in NCI-H358 tumours 2 h after a single dose of vehicle (black bar) or AMG 510 (blue bars). AMG 510 concentrations in plasma (red triangles) or tumours (black open circles). Data are mean  $\pm$  s.e.m.,  $n = 3$  mice per group; \*\*\* $P < 0.0001$ ; one-way analysis of variance (ANOVA) followed by Dunnett's multiple-comparison test. **b**, AMG 510 treatment results in covalent modification of KRAS(G12C), which inversely correlates with p-ERK inhibition in NCI-H358 tumours. Data are mean  $\pm$  s.d.,  $n = 3$  mice per group. **c-f**, Mice with established MIA PaCa-2 T2 tumours (**c**), NCI-H358 tumours (**d**), colorectal-cancer patient-derived xenografts (CRC PDX; **e**) or CT-26 KRAS<sup>G12C</sup> tumours (**f**) were treated with AMG 510. Data are mean  $\pm$  s.e.m.,  $n = 10$  mice per group, except for **e**,  $n = 8$  mice per group; \*\*\*\* $P < 0.0001$ , \* $P < 0.05$  compared with vehicle; repeated-measures ANOVA followed by Dunnett's multiple-comparison test;  $^{\#}P < 0.05$  regression by two-sided Student's *t*-test. **g-h**, Individual CT-26 KRAS<sup>G12C</sup> tumour volume plots from mice treated with 100  $\text{mg kg}^{-1}$  AMG 510 (**g**) or 200  $\text{mg kg}^{-1}$  AMG 510 (**h**) ( $n = 10$  per group).

For further evaluation of the signalling effect of KRAS(G12C) inhibition, two cell lines were treated with a titration of AMG 510 for 4 or 24 h, and signalling nodes were analysed by immunoblot (Extended Data Fig. 2b). The KRAS species shifted mobility upon the formation of covalent adducts with AMG 510 and accumulated with increasing time and dose, consistent with downstream inhibition of the MAPK pathway (that is, p-MEK1/2 and p-ERK1/2) in both cell lines (Extended Data Fig. 2b). KRAS(G12C) inhibition by AMG 510 also led to an accumulation of active EGFR (p-EGFR(Y1068)). Inhibition of AKT phosphorylation (p-AKT) was apparent in one cell line, whereas a decrease in S6 phosphorylation (p-S6) and an increase in cleaved caspase-3 were observed at 24 h in both lines, suggesting induction of apoptosis. In time course studies, treatment with AMG 510 at 0.1  $\mu\text{M}$  (Extended Data Fig. 2c) elicited rapid (<2 h) and sustained (>24 h) effects on MAPK and EGFR pathway signalling, whereas p-S6 and caspase cleavage emerged 8–16 h after treatment in both lines. To assess activity and selectivity, AMG 510 was profiled in 22 cell lines that had heterozygous or homozygous KRAS<sup>G12C</sup>, KRAS mutations other than KRAS<sup>G12C</sup> or wild-type KRAS. Treatment with AMG 510 for 2 h showed that basal p-ERK was inhibited in all KRAS<sup>G12C</sup> cell lines, with IC<sub>50</sub> values ranging from 0.010  $\mu\text{M}$  to 0.123  $\mu\text{M}$  (Fig. 1d and Supplementary Table 1). AMG 510 did not inhibit p-ERK in any of the non-KRAS<sup>G12C</sup> lines (IC<sub>50</sub> > 10  $\mu\text{M}$ ; Fig. 1d and Supplementary Table 1). In cell-viability assays, AMG 510 impaired the growth of all KRAS<sup>G12C</sup> cell lines, except SW1573, with IC<sub>50</sub> values ranging from 0.004  $\mu\text{M}$  to 0.032  $\mu\text{M}$  (Fig. 1e and Supplementary Table 1). Non-KRAS<sup>G12C</sup> lines were insensitive to AMG 510 (IC<sub>50</sub> > 7.5  $\mu\text{M}$ ; Fig. 1e and Supplementary Table 1). As reported for other KRAS(G12C) inhibitors<sup>4,5</sup>, spheroid growth conditions enhanced the sensitivity of most tested lines to AMG 510 (Extended Data Fig. 2d and Supplementary Table 1). To further determine the selectivity of the covalent interaction of AMG 510 with KRAS(G12C) and to identify other potential 'off-target' cellular proteins, cysteine-proteome profiling by mass spectrometry was performed as previously described<sup>4</sup>. After 4-h treatment with DMSO or 1  $\mu\text{M}$  AMG 510 (>30-fold above p-ERK IC<sub>50</sub>), the

cysteine proteome was enriched and peptides were identified. Among 6,451 unique cysteine-containing peptides, the Cys12 peptide from KRAS(G12C) was the only peptide that met the criteria for covalent target engagement<sup>4</sup> (Fig. 1f and Supplementary Table 2).

The effect of AMG 510 treatment on KRAS(G12C) signalling *in vivo* was evaluated in pharmacodynamics assays in which p-ERK was measured. In three KRAS<sup>G12C</sup> tumour models, AMG 510 inhibited p-ERK in a dose-dependent manner 2 h after treatment (Fig. 2a and Extended Data Fig. 3a, b) and maximal inhibition was observed at 30–100  $\text{mg kg}^{-1}$ . Time-course pharmacodynamics assays demonstrated peak plasma and tumour exposure of AMG 510 0.5 h after a single dose (10  $\text{mg kg}^{-1}$ ), leading to maximal inhibition of p-ERK 2–4 h after treatment and sustained inhibition for 48 h (Extended Data Fig. 3c, d). This was consistent with covalent inhibition of the long-lived KRAS(G12C) protein ( $t_{1/2} \approx 20$ –24 h; Extended Data Fig. 3e). Occupancy of KRAS(G12C) by AMG 510 was also measured by mass spectrometry and approached 100% at 100  $\text{mg kg}^{-1}$ , correlating with maximal suppression of p-ERK (Fig. 2b and Extended Data Fig. 3f). Time-course studies indicated that occupancy was detected by 0.5 h and maximal at 2 h (Extended Data Fig. 3g).

## Mutant-selective tumour inhibition *in vivo*

In mice with xenografts of human tumour cells, AMG 510 significantly inhibited the growth of MIA PaCa-2 T2 and NCI-H358 tumours at all doses, and regression of tumours was observed at higher doses (Fig. 2c, d). The dose of AMG 510 that was required to achieve the regression of MIA PaCa-2 T2 tumours was at least 3.3-fold lower than ARS-1620 (Extended Data Fig. 4a). Plasma exposures above the cellular IC<sub>90</sub> of p-ERK for more than 2 h resulted in tumour regression (Extended Data Fig. 4b, c). AMG 510 also inhibited the growth of KRAS<sup>G12C</sup>-mutant patient-derived xenografts (Fig. 2e and Extended Data Fig. 4d). By contrast, AMG 510 treatment had no effect on KRAS<sup>G12V</sup> tumour growth (Extended Data Fig. 4e). In immune-competent mice, AMG 510 resulted in regression of CT-26

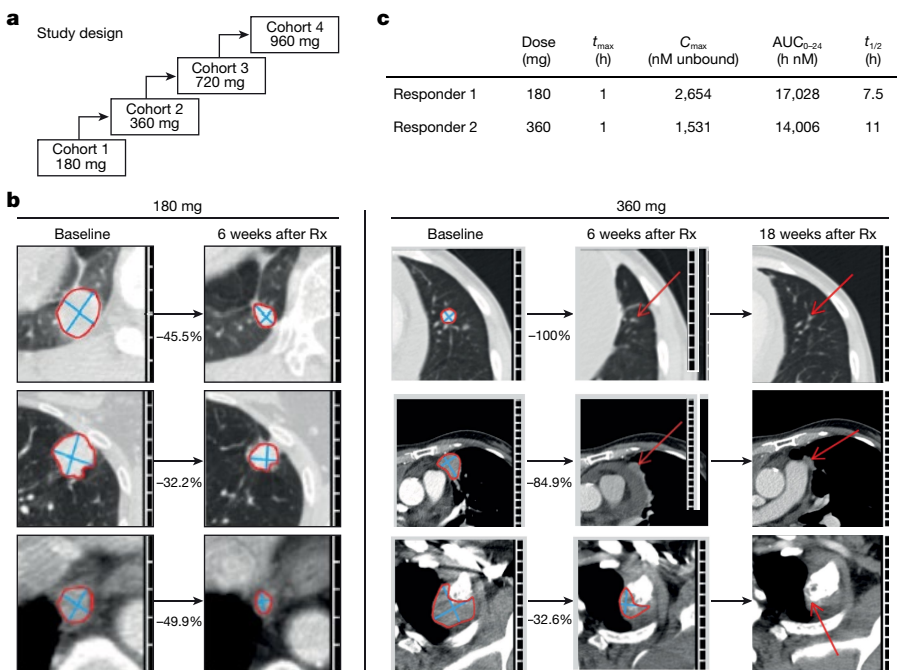


**Fig. 3 | Clinical activity of AMG 510 in patients with lung cancer in first-in-human dose-escalation study.** **a**, Study design. **b**, Computed tomography scans of patients with *KRAS*<sup>G12C</sup> lung carcinoma treated with AMG 510 (left, 180 mg; right, 360 mg). Representative pre-treatment (baseline) and post-treatment ( $R_x$ ) scans. Lesions are outlined by a red outline or highlighted by red

arrows. Left images show the lower-right lobe of the lungs (top), upper-left lobe of the lungs (middle) and lymph node (bottom). Right images show the upper left lobe of the lungs (top) and pleura (middle and bottom). Lesions in the 18-week scans of the patient who received 360 mg AMG 510 were considered too small to accurately measure. **c**, Pharmacokinetic data from the two responders.

*KRAS*<sup>G12C</sup> tumours, a mouse syngeneic tumour model generated by CRISPR technology (Fig. 2f). Two of the ten mice in the 100 mg kg<sup>-1</sup> group had no detectable tumours at the end of the study (day 29). However, regression of the tumours lacked durability (Fig. 2g), possibly owing to incomplete inhibition of p-ERK (Extended Data Fig. 3b). Therefore, a dose of 200 mg kg<sup>-1</sup> of AMG 510 was evaluated, resulting in near-complete inhibition of p-ERK (Extended Data Fig. 3b) and durable cures in eight out of ten mice (Fig. 2h), in which AMG 510 plasma levels were just below the cellular IC<sub>90</sub> (Extended Data Fig. 4f). Intriguingly, in the same tumour model but in mice that lacked T cells, AMG 510 induced regression but not cures, suggesting that the immune system drives cures in immune-competent mice (Extended Data Fig. 4g).

## Evidence of clinical activity

The enhanced potency and efficacy of AMG 510 prompted its selection as, to our knowledge, the first KRAS(G12C) inhibitor to enter clinical trials (clinicaltrials.gov identifier NCT03600883)<sup>16</sup>. AMG 510 was administered orally, once daily, in escalating dosing cohorts (Fig. 3a). In the first two dosing cohorts there were four patients with non-small-cell lung carcinoma (180 mg,  $n=3$ ; 360 mg,  $n=1$ ). Treatment with AMG 510 resulted in objective partial responses (as per RECIST1.1) in two patients (Fig. 3b and Extended Data Fig. 5) and stable disease in two patients. The two patients with a partial response had progressed on multiple previous systemic treatments including carboplatin, pemetrexed and nivolumab with documented disease progression. After 6 weeks of treatment with AMG 510, the first responder (180 mg) exhibited tumour shrinkage of 34%, and the second (360 mg) exhibited a tumour reduction of 67%. A follow-up scan at 18 weeks revealed complete resolution of target lesions in the second responder. AMG 510 exposures in both patients were above the cellular IC<sub>90</sub> of p-ERK (165 nM in MIA PaCa-2; Extended Data Fig. 4b) for 24 h (Fig. 3c). These patients remain active on AMG 510 treatment with the durations of 42 and 29 weeks, respectively, as of the cut-off date for the present data. We show that these patients responded to a

mutant-specific KRAS inhibitor, representing a milestone for patients with *KRAS*<sup>G12C</sup>-mutant cancer.

## AMG 510 improves efficacy of targeted agents

The clinically validated strategy of combining BRAF and MEK inhibitors<sup>22</sup> suggests that the combinations of AMG 510 and other inhibitors in the MAPK (and AKT) signalling pathways might enhance tumour-cell killing and overcome resistance. Therefore, *in vitro* combination experiments were conducted in several *KRAS*<sup>G12C</sup> cell lines with matrices of AMG 510 and inhibitors of HER kinases, EGFR, SHP2, PI3K, AKT and MEK (Extended Data Fig. 6a and Supplementary Table 3). As suggested by the induction of p-EGFR by AMG 510 (Extended Data Fig. 2b), the combination of AMG 510 with multiple agents resulted in synergistic killing<sup>23</sup> of NCI-H358 tumour cells (Fig. 4a, Extended Data Fig. 6a and Supplementary Table 3). Synergy was more limited in other lines, but the combination with a MEK inhibitor was synergistic in multiple settings and was enhanced in spheroid growth conditions (Fig. 4a). Significantly enhanced anti-tumour activity was also observed *in vivo* with a minimally efficacious dose of AMG 510 in combination with a MEK inhibitor, when compared to either of the single agents alone (Fig. 4b). These data suggest that the clinical combination of AMG 510 with MAPK inhibitors might eliminate bypass or residual signalling that could limit efficacy or induce resistance.

Given the prevalence of *KRAS*<sup>G12C</sup> in lung adenocarcinoma, a combination treatment of AMG 510 with carboplatin, a standard-of-care chemotherapeutic, was investigated. Treatment with either AMG 510 or carboplatin resulted in significant inhibition of NCI-H358 tumour growth in mice (Fig. 4c). However, combination treatment at various doses resulted in significantly improved anti-tumour efficacy (Fig. 4c and Extended Data Fig. 6b). The demonstration of enhanced efficacy of the combination of a mutant-selective KRAS inhibitor and a chemotherapeutic agent provides rationale for this approach in the clinic.

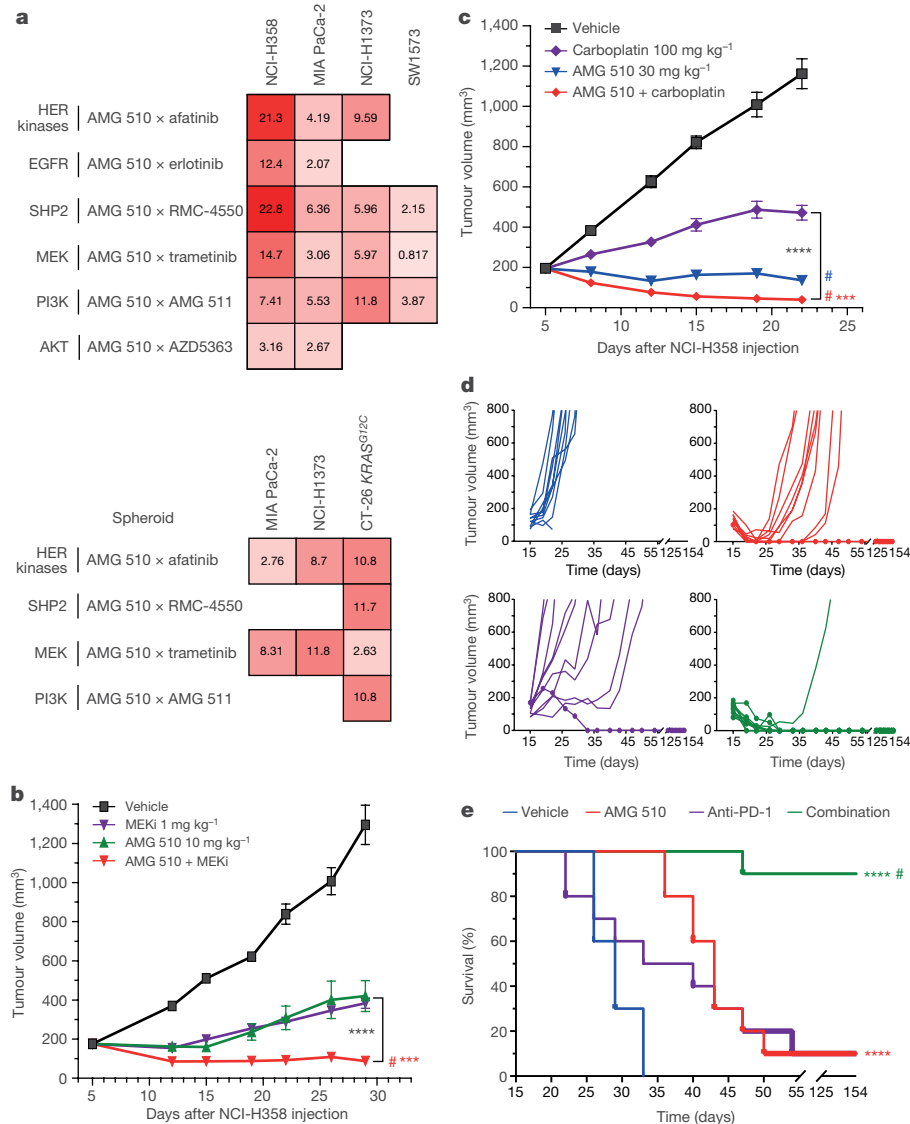


**Fig. 4 | AMG 510 combined with cytotoxic or targeted agents results in enhanced efficacy.** **a**, Synergy scores for AMG 510 combinations with targeted agents represented as a heat map, with higher scores (darker red) denoting stronger synergy. **b**, AMG 510 in combination with a MEK inhibitor (PD-0325901). **c**, AMG 510 in combination with carboplatin. **d**, CT-26 KRAS<sup>G12C</sup> tumour growth in individual mice. Lines with circles indicate tumour-free mice. **e**, Kaplan–Meier analysis of survival end point (tumour size  $> 800 \text{ mm}^3$ ). **b, c**, Data are

mean  $\pm$  s.e.m.,  $n = 10$  mice per group; \*\*\* $P \leq 0.001$  for combination treatment compared with the single agent; \*\*\*\* $P < 0.0001$  for treatment group compared with vehicle;  $P$  values were determined by repeated-measures ANOVA followed by Dunnett's multiple-comparison test; # $P < 0.001$  regression by two-sided Student's  $t$ -test. **e**,  $n = 10$  mice per group; \*\*\*\* $P < 0.0001$  compared with vehicle; # $P < 0.001$  combination versus AMG 510 or anti-PD-1 determined by two-sided Mantel–Cox test.

## AMG 510 synergizes with immunotherapy

Blockade of the immune checkpoint axis that involves programmed cell death 1 (PD-1)–programmed death ligand 1 (PD-L1) is clinically validated in multiple settings. As the long term cures induced by AMG 510 in the CT-26 KRAS<sup>G12C</sup> model were dependent on the engagement of the immune system (Fig. 2h and Extended Data Fig. 4g), strategies such as anti-PD-1 therapy that further boost anti-tumour T cell activity may synergize with AMG 510. The CT-26 KRAS<sup>G12C</sup> model is dependent on the KRAS<sup>G12C</sup> allele (Extended Data Fig. 7a, b) and is sensitive to AMG 510 treatment (Fig. 2f and Extended Data Fig. 3b). Furthermore, its parental line CT-26 has been broadly used to evaluate the effects of immunotherapy as well as combinations of immunotherapeutic and targeted agents<sup>24–26</sup>. Therefore, we used this model to evaluate the combination of anti-PD-1 immune checkpoint inhibition with AMG 510, which was administered at a suboptimal dose to enable the evaluation of combination effects. As shown above (Fig. 2f, g), AMG 510 caused tumour regression in mice as a single agent (Fig. 4d),

but only one out of ten tumours remained completely regressed (Fig. 4d). Anti-PD-1 monotherapy delayed tumour growth, with complete regression in only one of ten tumours. Notably, combined treatment led to complete responses in nine out of ten mice (Fig. 4d). Treatment was stopped after day 43, and all complete responders remained cured 112 days later. Using a surrogate end point (tumour volume  $> 800 \text{ mm}^3$ ), the combined treatment significantly improved survival (Fig. 4e).

To understand the effects of treatment on immune cell composition, CT-26 KRAS<sup>G12C</sup> tumours were immunophenotyped. After 4 days of treatment, AMG 510 markedly increased the infiltration of T cells, primarily CD8<sup>+</sup> T cells, into the tumour (Fig. 5a and Extended Data Fig. 8a). Increased infiltration of CD8<sup>+</sup> T cells was also observed in the combination group, but not after anti-PD-1 monotherapy. Immunohistochemical analysis also revealed an increased number of total and proliferating CD3<sup>+</sup> T cells and total CD8<sup>+</sup> T cells after AMG 510 treatment, which were further increased after the combination treatment (Fig. 5b, c). As an

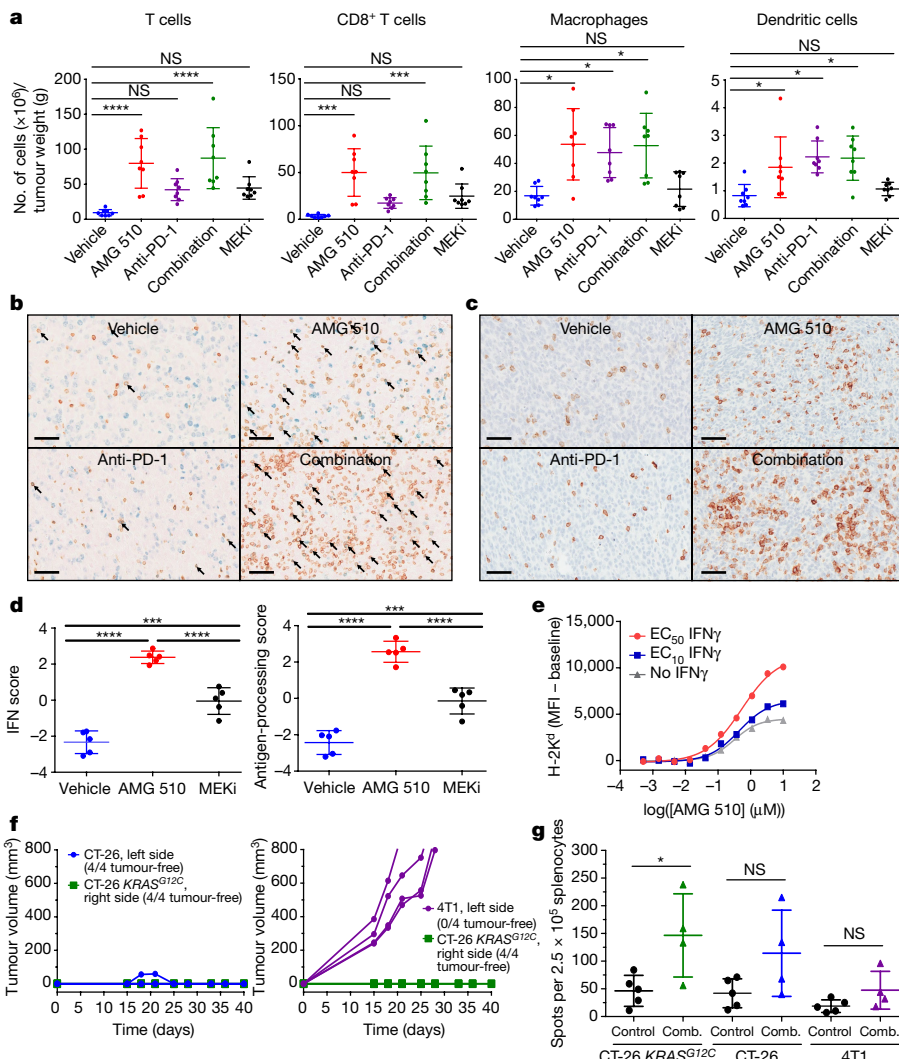


**Fig. 5 | AMG 510 treatment induces a pro-inflammatory tumour microenvironment.** **a–c**, CT-26 KRAS<sup>G12C</sup> tumours were immunophenotyped by flow cytometry (**a**) or immunohistochemistry of CD3 and Ki-67 (**b**) or CD8 (**c**). **a**,  $n=8$  per group; **b, c**,  $n=5$  per group. Ki-67 is shown in blue and has a nuclear localization; CD3 and CD8 stains are shown in brown and are cytoplasmic. Arrows in **b** highlight examples that are double-positive for CD3 and Ki-67. Scale bars, 50  $\mu\text{m}$ . **d**, RNA was isolated from CT-26 KRAS<sup>G12C</sup> tumours ( $n=5$  per group). Gene expression and scores were calculated by NanoString technology. **e**, Cell surface expression of MHC class I antigen H-2K<sup>d</sup> on CT-26 KRAS<sup>G12C</sup> cells that were treated with AMG 510 together with or without IFN $\gamma$  as measured by flow cytometry. **f**, Individual tumour growth in mice that were cured with AMG 510 and anti-PD-1 treatment and were then rechallenged with CT-26 KRAS<sup>G12C</sup>, CT-26 or 4T1 cells. **g**, Splenocytes were collected and challenged with CT-26, CT-26 KRAS<sup>G12C</sup> or 4T1 cells. Levels of secreted IFN $\gamma$  were measured by ELISpot assay.  $n=5$  control,  $n=4$  combination. **a, d, g**, Data are mean  $\pm$  s.d. **a, d**, \*\*\*\* $P<0.0001$ , \*\*\* $P<0.001$ , \* $P<0.05$ ; NS, not significant; one-way ANOVA followed by Tukey's test. **g**, \* $P=0.0269$ ; two-sided Student's *t*-test.

additional comparison we used a MEK inhibitor, which blocked MAPK signalling downstream of RAS (Extended Data Fig. 8b). This inhibitor regressed CT-26 KRAS<sup>G12C</sup> tumours in mice to a similar level as AMG 510 (Extended Data Fig. 8c, d), but did not significantly affect the numbers of infiltrating CD8<sup>+</sup> T cells (Fig. 5a). AMG 510 treatment also increased the infiltration of macrophages and dendritic cells, including CD103<sup>+</sup> cross-presenting dendritic cells, which are critical for T cell priming and activation and are implicated in T cell recruitment<sup>27</sup> (Fig. 5a and Extended Data Fig. 8a). PD-1 expression on CD8<sup>+</sup> T cells was moderately increased by both AMG 510 and the MEK inhibitor (Extended Data Fig. 8a).

Tumour RNA was purified after 2 days of treatment for transcriptional profiling of a panel of immune-associated genes. AMG 510 induced a pro-inflammatory microenvironment characterized by increased interferon signalling, chemokine production, antigen processing, cytotoxic and natural killer cell activity, as well as markers of innate immune system stimulation, that were significantly higher compared to the effects induced by MEK inhibition (Fig. 5d and Extended Data Fig. 8e). Infiltration of immune cells was correlated with increased expression of several chemokines including Cxcl11 (Extended Data Fig. 8e and Supplementary Table 4). To examine whether these immune-enhancing effects were directly attributable to AMG 510, CT-26 KRAS<sup>G12C</sup> cells were treated with AMG 510 in vitro and the expression of immune genes was measured. AMG 510 induced expression of Cxcl10 and Cxcl11 (Extended Data Fig. 9a), which are key attractants of tumour-suppressive immune cells<sup>27,28</sup>. This provides a potential mechanistic link by which AMG 510 treatment increases the intratumoral concentration of chemokines, leading to the infiltration of T cells and dendritic cells and improved immunosurveillance.

Previous data suggested that although MEK inhibition could promote anti-tumour activity in combination with anti-PD-L1 treatment *in vivo*, it can also inhibit T cell function<sup>24</sup>. Using an *in vitro* co-culture system with mouse bone marrow-derived dendritic cells and transgenic CD8<sup>+</sup> T cells, MEK inhibition impaired antigen-specific T cell proliferation, whereas AMG 510 did not affect the T cell response (Extended Data Fig. 9b). Furthermore, AMG 510 induced expression of MHC class I antigens on CT-26 KRAS<sup>G12C</sup> tumour cells *in vitro* (Fig. 5e and Extended Data Fig. 9c). These data suggest that AMG 510 treatment leads to increased T cell priming, antigen recognition of tumour cells and the potential establishment of long-term anti-tumour T cell responses. To test this, mice that were cured by the combined treatment of AMG 510 and anti-PD-1 (Fig. 4d) were rechallenged with bilateral tumours of CT-26 KRAS<sup>G12C</sup> and parental CT-26 (KRAS<sup>G12D</sup>) cells, or CT-26 KRAS<sup>G12C</sup> and an unrelated mouse breast tumour model, 4T1. All 4T1 tumours (four out of four) grew, but none of the CT-26 KRAS<sup>G12C</sup> tumours (zero out of eight) or CT-26 parental tumours (zero out of four) became established (Fig. 5f). In a control group of naive mice, all parental CT-26 and CT-26 KRAS<sup>G12C</sup> tumours grew (15 out of 15; Extended Data Fig. 9d). Splenocytes collected from the cured mice were stimulated with CT-26, CT-26 KRAS<sup>G12C</sup> or 4T1 tumour cells, and we measured secreted IFN $\gamma$  as a marker of tumour-specific T cell priming and activity. CT-26 KRAS<sup>G12C</sup> cells and parental CT-26 cells caused nearly a threefold increase in IFN $\gamma$ , which was not induced by 4T1 cells (Fig. 5g). Together, these data suggest that the combination of AMG 510 and anti-PD-1 therapy prompted the establishment of long-term tumour-specific T cell responses.

## Discussion

The discovery of the interaction with the His95 groove of KRAS(G12C) enabled markedly increased potency and the identification of AMG 510, a first-in-class oral KRAS(G12C) inhibitor with evidence of clinical activity in patients with *KRAS<sup>G12C</sup>* mutant cancer. Preclinically, AMG 510 selectively targeted *KRAS<sup>G12C</sup>* tumours, caused durable regression as a monotherapy, and could be combined with cytotoxic and targeted agents to synergistically kill tumour cells. AMG 510 treatment led to an inflamed tumour microenvironment that was highly responsive to immune-checkpoint inhibition. Combined treatment of anti-PD-1 therapy and a MEK inhibitor has shown preclinical efficacy in several reports<sup>24,29,30</sup>, and this was associated with increased T cell infiltration. In the present study, significantly greater immune cell infiltration was observed after selective KRAS(G12C) inhibition compared to the MEK inhibitor. In contrast to the reported effects of non-tumour-selective MEK inhibition, which blocks T cell expansion and priming<sup>24</sup>, selective inhibition of KRAS(G12C) by AMG 510 resulted in increased T cell infiltration and activation. Furthermore, the combination of AMG 510 and anti-PD-1 therapy established a memory T cell response against both the CT-26 *KRAS<sup>G12C</sup>* cells and the parental CT-26 tumour cells. These data support a model of enhanced antigen recognition and T cell memory in which AMG 510-induced tumour cell death and innate immune responses, combined with anti-PD-1 treatment, results in an adaptive immune response that can recognize and eradicate related but non-*KRAS<sup>G12C</sup>* tumours. There is ample evidence that the intratumoral KRAS mutation status can be heterogeneous within the same tumour and between primary and metastatic sites<sup>31–33</sup>. Taken together, our data suggest that AMG 510 might be an effective anti-tumour agent even in settings in which *KRAS<sup>G12C</sup>* expression is heterogenous.

## Reporting summary

Further information on research design is available in the Nature Research Reporting Summary linked to this paper.

## Data availability

Most of the data generated or analysed during this study are included in this published Article or available as Source Data. X-ray crystallographic coordinates and structure factor files have been deposited in the Protein Data Bank (PDB: 6OIM). Other data that support the findings of this study are available from the corresponding authors. Qualified researchers may request data from Amgen clinical studies. Further details are available at <http://www.amgen.com/datasharing>.

## Online content

Any methods, additional references, Nature Research reporting summaries, source data, extended data, supplementary information, acknowledgements, peer review information; details of author contributions and competing interests; and statements of data and code availability are available at <https://doi.org/10.1038/s41586-019-1694-1>.

- Barbacid, M. *ras genes*. *Annu. Rev. Biochem.* **56**, 779–827 (1987).
- Simanshu, D. K., Nissley, D. V. & McCormick, F. RAS proteins and their regulators in human disease. *Cell* **170**, 17–33 (2017).
- Ostrem, J. M., Peters, U., Sos, M. L., Wells, J. A. & Shokat, K. M. K-Ras(G12C) inhibitors allosterically control GTP affinity and effector interactions. *Nature* **503**, 548–551 (2013).

- Patricelli, M. P. et al. Selective inhibition of oncogenic KRAS output with small molecules targeting the inactive state. *Cancer Discov.* **6**, 316–329 (2016).
- Janes, M. R. et al. Targeting KRAS mutant cancers with a covalent G12C-specific inhibitor. *Cell* **172**, 578–589 (2018).
- Pai, E. F. et al. Structure of the guanine-nucleotide-binding domain of the Ha-ras oncogene product p21 in the triphosphate conformation. *Nature* **341**, 209–214 (1989).
- Milburn, M. V. et al. Molecular switch for signal transduction: structural differences between active and inactive forms of protooncogenic ras proteins. *Science* **247**, 939–945 (1990).
- Culty, M. & Downward, J. SnapShot: Ras signaling. *Cell* **133**, 1292–1292.e1 (2008).
- Vetter, I. R. & Wittinghofer, A. The guanine nucleotide-binding switch in three dimensions. *Science* **294**, 1299–1304 (2001).
- Scheffzek, K. et al. The Ras-RasGAP complex: structural basis for GTPase activation and its loss in oncogenic Ras mutants. *Science* **277**, 333–338 (1997).
- Jimeno, A., Messersmith, W. A., Hirsch, F. R., Franklin, W. A. & Eckhardt, S. G. KRAS mutations and susceptibility to cetuximab and panitumumab in colorectal cancer. *Cancer J.* **15**, 110–113 (2009).
- Welsch, S. J. & Corrie, P. G. Management of BRAF and MEK inhibitor toxicities in patients with metastatic melanoma. *Ther. Adv. Med. Oncol.* **7**, 122–136 (2015).
- Fakih, M. & Vincent, M. Adverse events associated with anti-EGFR therapies for the treatment of metastatic colorectal cancer. *Curr. Oncol.* **17**, S18–S30 (2010).
- AACR Project GENIE Consortium. AACR Project GENIE: powering precision medicine through an international consortium. *Cancer Discov.* **7**, 818–831 (2017).
- Hansen, R. et al. The reactivity-driven biochemical mechanism of covalent KRAS<sup>G12C</sup> inhibitors. *Nat. Struct. Mol. Biol.* **25**, 454–462 (2018).
- [clinicaltrials.gov. A Phase 1/2, Study Evaluating the Safety, Tolerability, PK, and Efficacy of AMG 510 in Subjects With Solid Tumors With a Specific KRAS Mutation https://clinicaltrials.gov/ct2/show/NCT03600883](https://clinicaltrials.gov/ct2/show/NCT03600883) (2018).
- Gentile, D. R. et al. Ras binder induces a modified switch-II Pocket in GTP and GDP states. *Cell Chem. Biol.* **24**, 1455–1466 (2017).
- Schwartz, P. A. et al. Covalent EGFR inhibitor analysis reveals importance of reversible interactions to potency and mechanisms of drug resistance. *Proc. Natl. Acad. Sci. USA* **111**, 173–178 (2014).
- Cee, V. J. et al. Systematic study of the glutathione (GSH) reactivity of N-arylacrylamides: 1. Effects of aryl substitution. *J. Med. Chem.* **58**, 9171–9178 (2015).
- Jackson, P. A., Widen, J. C., Harki, D. A. & Brummond, K. M. Covalent modifiers: a chemical perspective on the reactivity of α,β-unsaturated carbonyls with thiols via hetero-Michael addition reactions. *J. Med. Chem.* **60**, 839–885 (2017).
- Nichols, R. J. et al. RAS nucleotide cycling underlies the SHP2 phosphatase dependence of mutant BRAF-, NF1- and RAS-driven cancers. *Nat. Cell Biol.* **20**, 1064–1073 (2018).
- Robert, C. et al. Improved overall survival in melanoma with combined dabrafenib and trametinib. *N. Engl. J. Med.* **372**, 30–39 (2015).
- Saiki, A. Y. et al. MDM2 antagonists synergize broadly and robustly with compounds targeting fundamental oncogenic signaling pathways. *Oncotarget* **5**, 2030–2043 (2014).
- Ebert, P. J. R. et al. MAP kinase inhibition promotes T cell and anti-tumor activity in combination with PD-L1 checkpoint blockade. *Immunity* **44**, 609–621 (2016).
- Selby, M. J. et al. Preclinical development of ipilimumab and nivolumab combination immunotherapy: mouse tumor models, in vitro functional studies, and cynomolgus macaque toxicology. *PLoS ONE* **11**, e0161779 (2016).
- Mosely, S. I. et al. Rational selection of syngeneic preclinical tumor models for immunotherapeutic drug discovery. *Cancer Immunol. Res.* **5**, 29–41 (2017).
- Spranger, S., Dai, D., Horton, B. & Gajewski, T. F. Tumor-residing Batf3 dendritic cells are required for effector T cell trafficking and adoptive T cell therapy. *Cancer Cell* **31**, 711–723 (2017).
- Gao, Q. et al. Cancer-cell-secreted CXCL11 promoted CD8<sup>+</sup> T cells infiltration through docetaxel-induced-release of HMGB1 in NSCLC. *J. Immunother. Cancer* **7**, 42 (2019).
- Lee, J. W. et al. The combination of MEK inhibitor with immunomodulatory antibodies targeting programmed death 1 and programmed death ligand 1 results in prolonged survival in *Kras*/p53-driven lung cancer. *Journal Thorac. Oncol.* **14**, 1046–1060 (2019).
- Liu, L. et al. The BRAF and MEK inhibitors Dabrafenib and Trametinib: Effects on Immune Function and in Combination with Immunomodulatory antibodies targeting PD-1, PD-L1, and CTLA-4. *Clin. Cancer Res.* **21**, 1639–1651 (2015).
- Kordiak, J. et al. Intratumor heterogeneity and tissue distribution of KRAS mutation in non-small cell lung cancer: implications for detection of mutated KRAS oncogene in exhaled breath condensate. *J. Cancer Res. Clin. Oncol.* **145**, 241–251 (2019).
- Lamy, A. et al. Metastatic colorectal cancer KRAS genotyping in routine practice: results and pitfalls. *Mod. Pathol.* **24**, 1090–1100 (2011).
- Richman, S. D. et al. Intra-tumoral heterogeneity of KRAS and BRAF mutation status in patients with advanced colorectal cancer (aCRC) and cost-effectiveness of multiple sample testing. *Anal. Cell. Pathol.* **34**, 61–66 (2011).

**Publisher's note** Springer Nature remains neutral with regard to jurisdictional claims in published maps and institutional affiliations.

© The Author(s), under exclusive licence to Springer Nature Limited 2019

# Article

**Acknowledgements** We thank N. Moua Vang, P. Achanta, J. Estrada, P. Mitchell, T. Tsuruda, D. Mohl, C. Liu, J. Lofgren, R. Shimanovich, P. Agarwal, R. S. Foti, Y. B. Yu, J. Yadav, M. Singh, J. Nam, C. Wang, R. Pham, W. Rufai, T. McElroy, S. Tiso, M. Farley, J. Ngang, D. Wu, R. Dawson, J. Reidy, J. Egen, R. Kendall, P. J. Beltran, M. Eschenberg, S. Caenepeel, P. Hughes, A. Coxon, F. Martin, P. K. Morrow, S. Agrawal, D. Nagorsen and G. Friberg for their support and contributions; all of the patients who participated in the AMG 510 first-in-human clinical trial; and the staff of Crystallographic Consulting and the Advanced Light Source at beamline 5.0.1 for their data collection support. The Berkeley Center for Structural Biology is supported in part by the National Institutes of Health, National Institute of General Medical Sciences and the Howard Hughes Medical Institute. The Advanced Light Source is supported by the Director, Office of Science, Office of Basic Energy Sciences, of the US Department of Energy under contract no. DE-AC02-05CH11231.

**Author contributions** B.A.L. oversaw the design and synthesis of compounds. C.M. solved the crystal structure of AMG 510. J.D.M. and T.A. designed the nucleotide-exchange assay and mass spectrometry experiment with recombinant KRAS, and T.S.M. and A.Y.S. developed the assays. L.P.V. and C.G.K. oversaw the bioanalytical assessment of AMG 510. J.-R.S., T.H., K.C., K.R., A.Y.S. and T.O. executed and analysed *in vivo* studies. L.P.V., X.Z. and R.O. developed methods, and N.K. quantified KRAS(G12C)–AMG 510 covalent adducts in cells and tumour samples. L.P.V., R.O. and X.Z. developed and executed the SILAC study to determine the half-life of KRAS(G12C). J.R.L., A.Y.S., T.A., W.O. and V.J.C. designed, and A.Y.S., T.S.M., A.S.R. and K.G. executed *in vitro* experiments. J.W. generated the immunohistochemical data. D.B. designed and analysed proteomic experiments. B.E.H. provided clinical pharmacokinetic data. J.C., K.R. and K.C. designed the *in vivo* experiments. H.H. oversaw the clinical development. M.G.F., B.H.O., T.J.P., G.S.F., J.D., J.K., R.G. and D.S.H. were investigators for the AMG 510 clinical trial. J.C., J.R.L., V.J.C., A.Y.S. and K.R. wrote the paper with contributions from all authors.

**Competing interests** J.C., K.R., A.Y.S., C.M., K.C., D.B., K.G., T.H., C.G.K., N.K., B.A.L., J.W., A.S.R., R.S.M., R.O., T.O., J.-R.S., X.Z., J.D.M., L.P.V., B.E.H., W.O., H.H., T.A., V.J.C. and J.R.L. were employees and stock holders of Amgen at the time of data collection. M.G.F. has received grant and research support from AstraZeneca, Amgen and Novartis; served as a consultant for Array BioPharma, Amgen and Seattle Genetics; and has been part of the speakers bureau for Amgen. B.H.O. has received honoraria from Amgen. T.J.P. has received grants and research support from Amgen. G.S.F. is employed by HealthONE and the Sarah Cannon Research

Institute; has served in a consulting or advisory capacity for EMD Serono and Fujifilm; has received research funding from 3-V Biosciences, Abbvie, ADC Therapeutics, Aileron, American Society of Clinical Oncology, Amgen, ARMO, AstraZeneca, BeiGene, Bioatla, Biothera, Celldex, Celgene, Ciclomed, Curegenix, Curis, DelMar, eFFECTOR, Eli Lilly, EMD Serono, Exelixis, Fujifilm, Genmab, GlaxoSmithKline, Hutchison MediPharma, Ignyta, Incyte, Jacobio, Jounce, KoltaN, Loxo, MedImmune, Millennium, Merck, Mirna Therapeutics, the National Institutes of Health, Novartis, OncoMed, OncoTherreon, Precision Oncology, Regeneron, Rgenix, Ribon, Strategia, Syndax, Taiho, Takeda, Tarveda, Tesaro, Tocagen, Turning Point Therapeutics, the UT MD Anderson Cancer Center and Vegenics; receives royalties from Wolters Kluwer; and has also received travel, accommodation and related expenses from Bristol-Myers Squibb, EMD Serono, Fujifilm, Millennium and the Sarah Cannon Research Institute. J.D. has served in a consulting or advisory capacity for Amgen, BeiGene, Biomics, Eisai, Eli Lilly and Novartis; and received research funding from Biomics, GlaxoSmithKline, Novartis and Roche. J.K. has received travel, accommodation and expenses from Bristol-Myers Squibb, MSD and Zucero Therapeutics. R.G. has served in a consulting or advisory capacity for AbbVie, Adaptimmune, AstraZeneca, Celgene, Ignyta, Invata, Merck, Nektar, Pfizer and Roche. D.S.H. has stock and other ownership interests in Molecular Match, OncoResponse and Presagia; has served in a consulting or advisory capacity for Alpha Insights, Axiom, Adaptimmune, Baxter, Bayer, Genentech, GLG, Group H, Guidepoint Global, Infinity, Janssen, Merrimack, Medscape, Numab, Pfizer, Seattle Genetics, Takeda and Trienza Therapeutics; has received research and/or grant funding from AbbVie, Adaptimmune, Amgen, AstraZeneca, Bayer, BMS, Daiichi-Sankyo, Eisai, Fate Therapeutics, Genentech, Genmab, Ignyta, Infinity, Kite, Kyowa, Eli Lilly, LOXO, Merck, MedImmune, Mirati, Mirna Therapeutics, Molecular Templates, Mologen, NCI-CTEP, Novartis, Pfizer, Seattle Genetics and Takeda; and has received travel, accommodation and expenses from Genmab, Loxo Oncology, ASCO, AACR, SITC and Mirna Therapeutics.

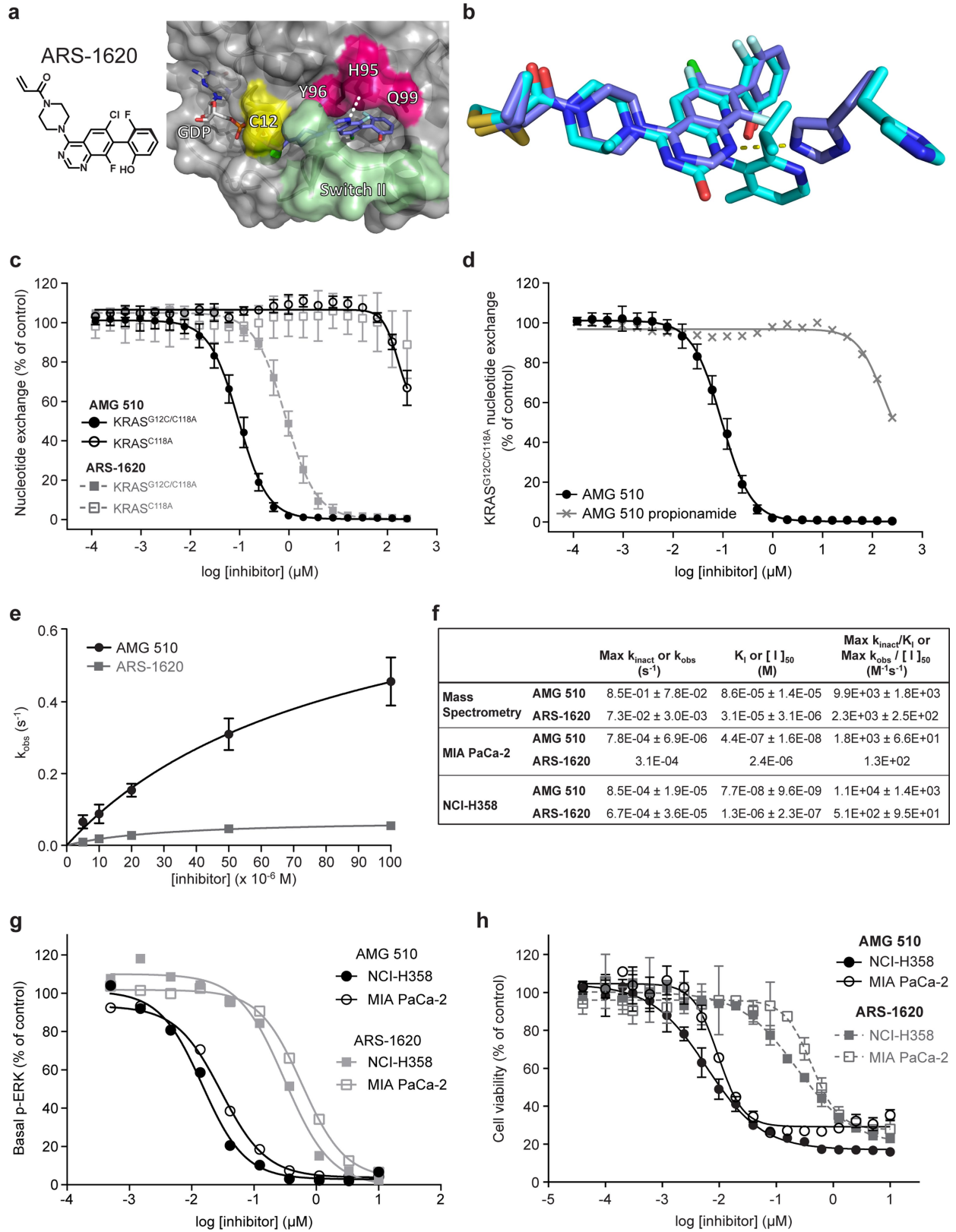
## Additional information

**Supplementary information** is available for this paper at <https://doi.org/10.1038/s41586-019-1694-1>.

**Correspondence and requests for materials** should be addressed to J.C. or J.R.L.

**Peer review information** *Nature* thanks Rene Bernards and the other, anonymous, reviewer(s) for their contribution to the peer review of this work.

**Reprints and permissions information** is available at <http://www.nature.com/reprints>.

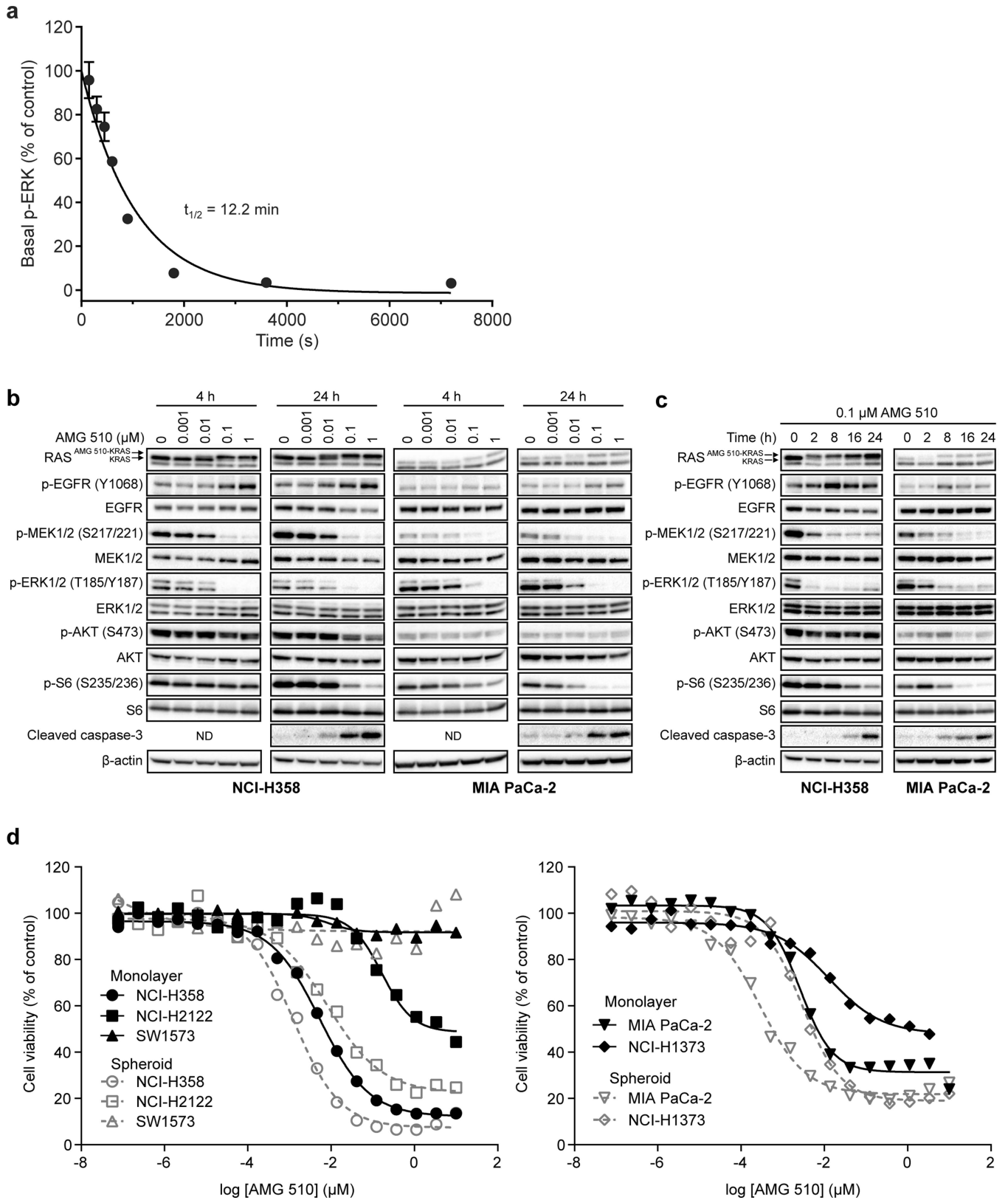


**Extended Data Fig. 1** | See next page for caption.

# Article

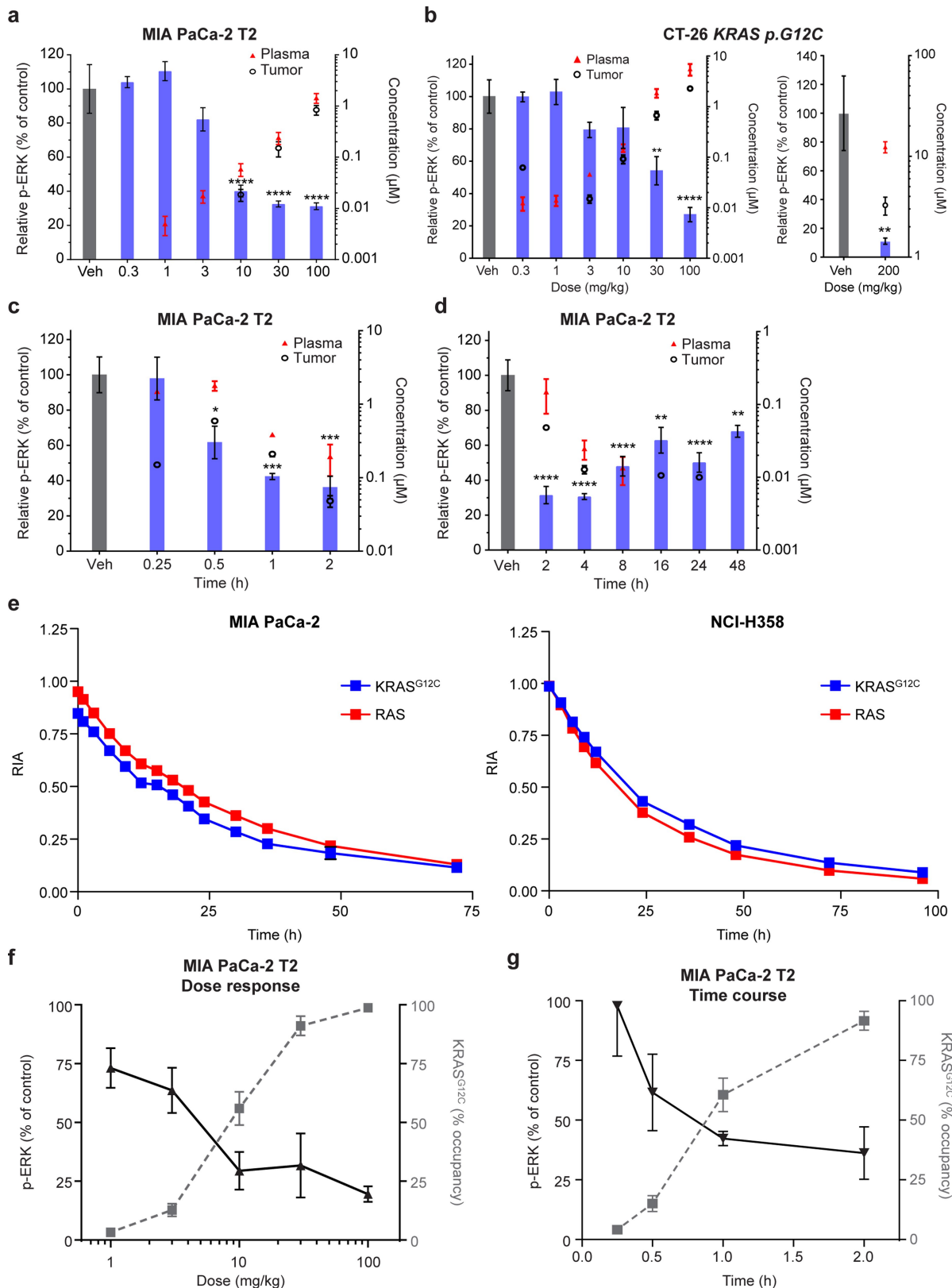
**Extended Data Fig. 1 | Enhanced binding of AMG 510 to KRAS(G12C) results in improved properties.** **a**, X-ray co-crystal structure of KRAS(G12C/C51S/C80L/C118S) bound to GDP and ARS-1620 (PDB: 5V9U). **b**, Overlay of ARS-1620 and AMG 510. The right side shows different orientations of His95 (H95) depending on the ligand. **c**, Biochemical activity of AMG 510 and ARS-1620 in a nucleotide-exchange assay with purified KRAS(G12C/C118A) or KRAS(C118A) protein. Data are mean  $\pm$  s.d.,  $n = 4$  replicates. The wild-type cysteine at position 118 was changed to alanine to avoid reactivity with non-Cys12 cysteines. **d**, Biochemical activity of AMG 510 and its non-reactive propionamide analogue

in a nucleotide-exchange assay with purified KRAS(G12C/C118A); propionamide, mean of  $n = 2$  replicates. **e**, Kinetic properties of AMG 510 and ARS-1620 as determined by mass spectrometry. **f**, Calculated maximal reaction rates ( $k_{inact}$  or  $k_{obs}$ ) and the concentrations that achieve a half-maximal rate ( $K_1$  or  $[I]_{50}$ ) of AMG 510 and ARS-1620. **g**, **h**, Inhibition of p-ERK after a 2-h treatment (**g**; mean,  $n = 2$  replicates) and effects on cell viability after 72-h treatment (**h**; mean  $\pm$  s.d.,  $n = 3$  replicates) with AMG 510 or ARS-1620.



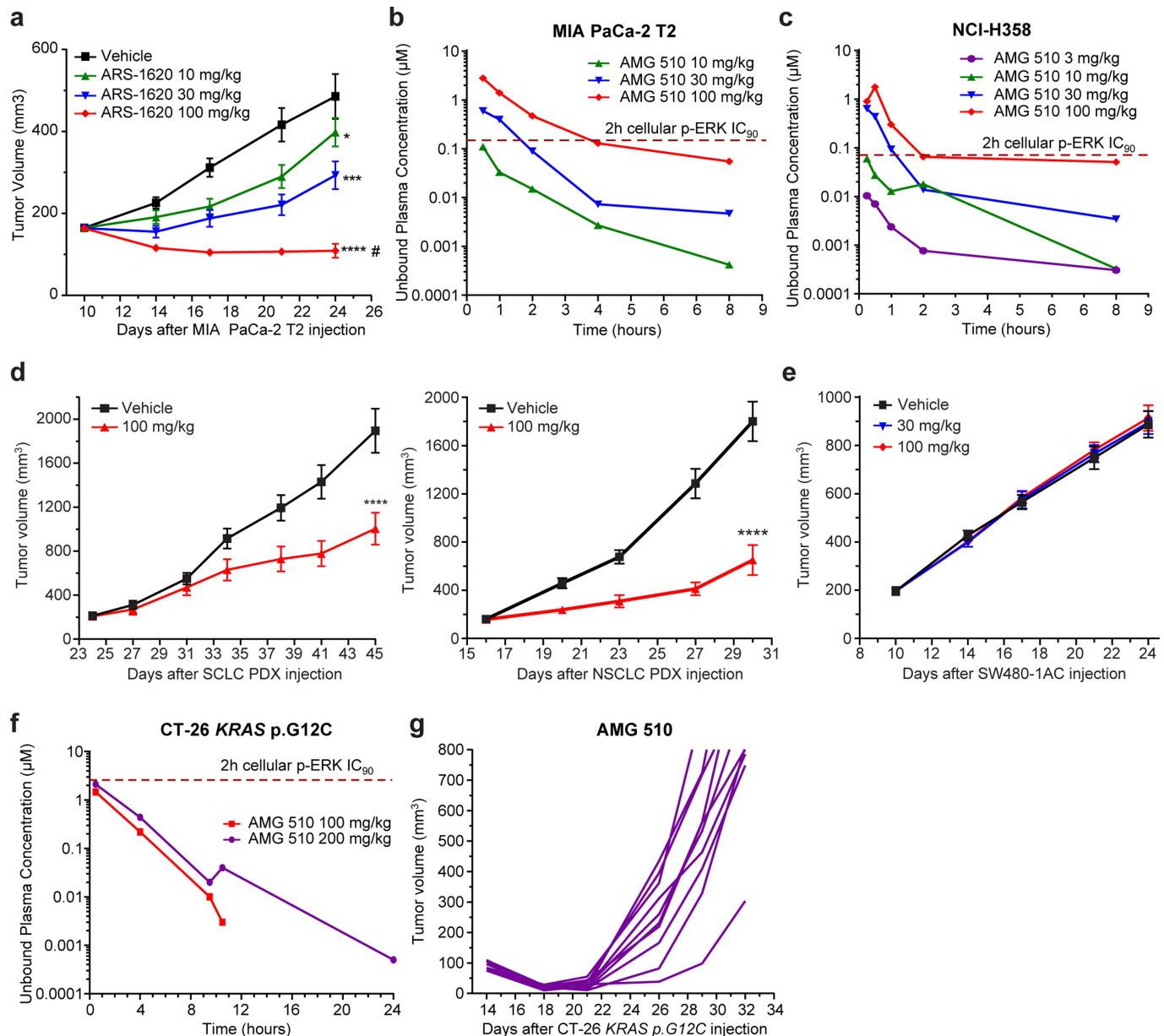
**Extended Data Fig. 2 | AMG 510 inhibits KRAS(G12C) signalling and impairs viability.** **a**, Inhibition of p-ERK with RMC-4550 in NCI-H358 cells. Data are mean  $\pm$  s.d.,  $n=3$  replicates. **b, c**, Effect on cellular signalling in NCI-H358 or MIA PaCa-2 after 4- or 24-h treatment with a serial titration of AMG 510 (**b**) or treatment with 0.1  $\mu\text{M}$  AMG 510 at time points for up to 24 h (**c**). Top arrow, AMG

510-KRAS(G12C) covalent adduct; bottom arrow, KRAS. Data are from a single experiment (Supplementary Fig. 1). **d**, Effect of 72-h treatment with AMG 510 on cell viability in adherent monolayer or spheroid culture conditions (mean,  $n=2$  replicates).



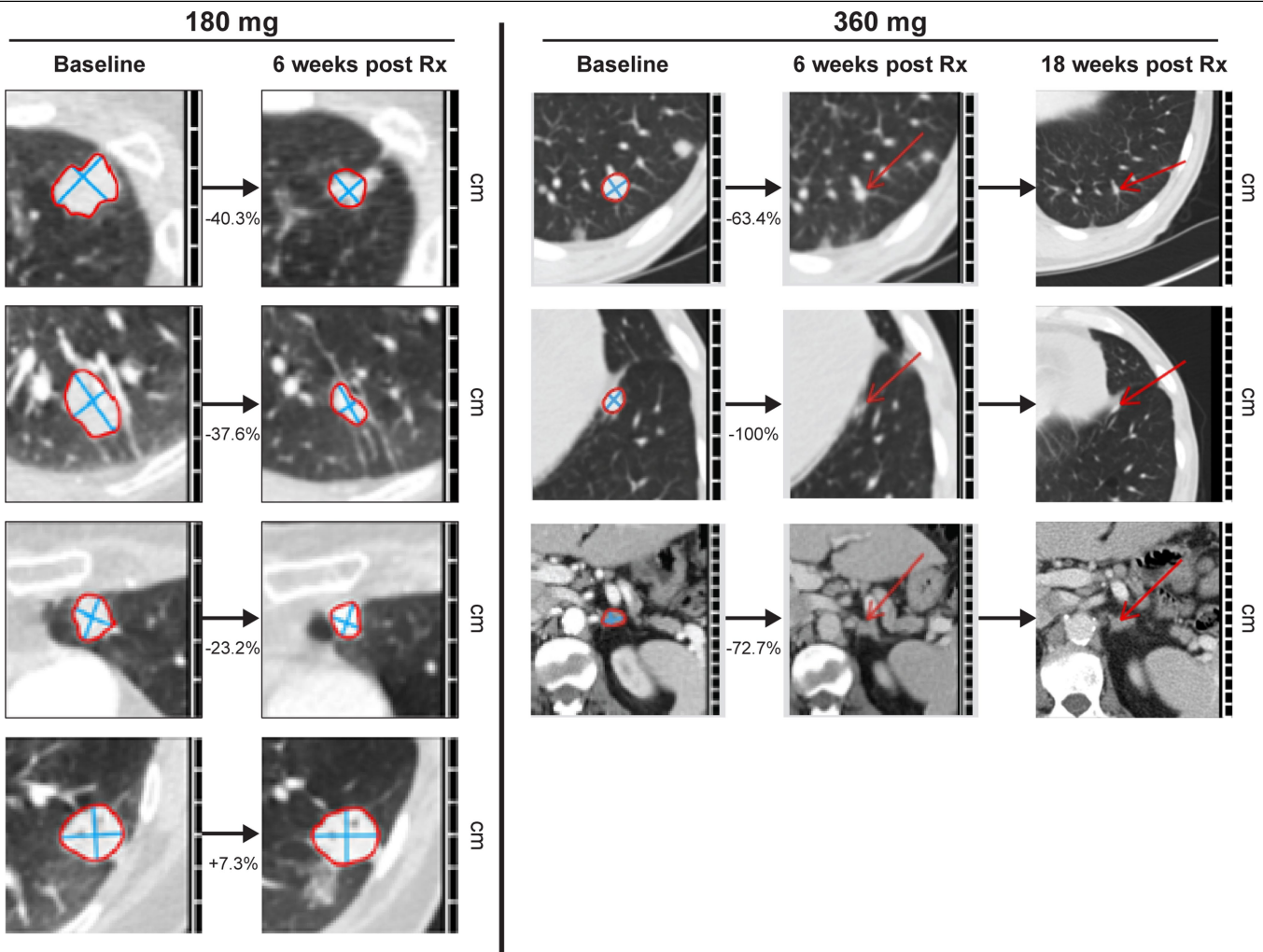
**Extended Data Fig. 3 | AMG 510 covalently modifies KRAS(G12C) in tumours and inhibits signalling in vivo.** **a–d**, Mice bearing MIA PaCa-2 T2 (**a, c, d**) or CT-26 KRAS<sup>G12C</sup> (**b**) tumours were treated orally with a single dose of vehicle (black bars) or with the indicated doses of AMG 510 (blue bars). Tumours were collected 2 h later (**a, b**) or over time as indicated (**c, d**) and levels of p-ERK were measured. AMG 510 concentrations in plasma (red triangles) or tumours (black open circles). Data are mean  $\pm$  s.e.m.,  $n = 3$  mice per group; \*\*\*\* $P < 0.0001$ , \*\*\* $P < 0.001$ ,

\*\* $P < 0.01$  compared with vehicle; one-way ANOVA followed by Dunnett's multiple-comparison test. **e**, Half-life determination of KRAS(G12C) in MIA PaCa-2 and NCI-H358 cells by SILAC. Data are mean  $\pm$  s.d.,  $n = 3$  replicates. **f, g**, AMG 510 treatment results in covalent modification of KRAS(G12C) that inversely correlates with p-ERK inhibition in MIA PaCa-2 T2 tumours. Data are mean  $\pm$  s.d.,  $n = 3$  mice per group.



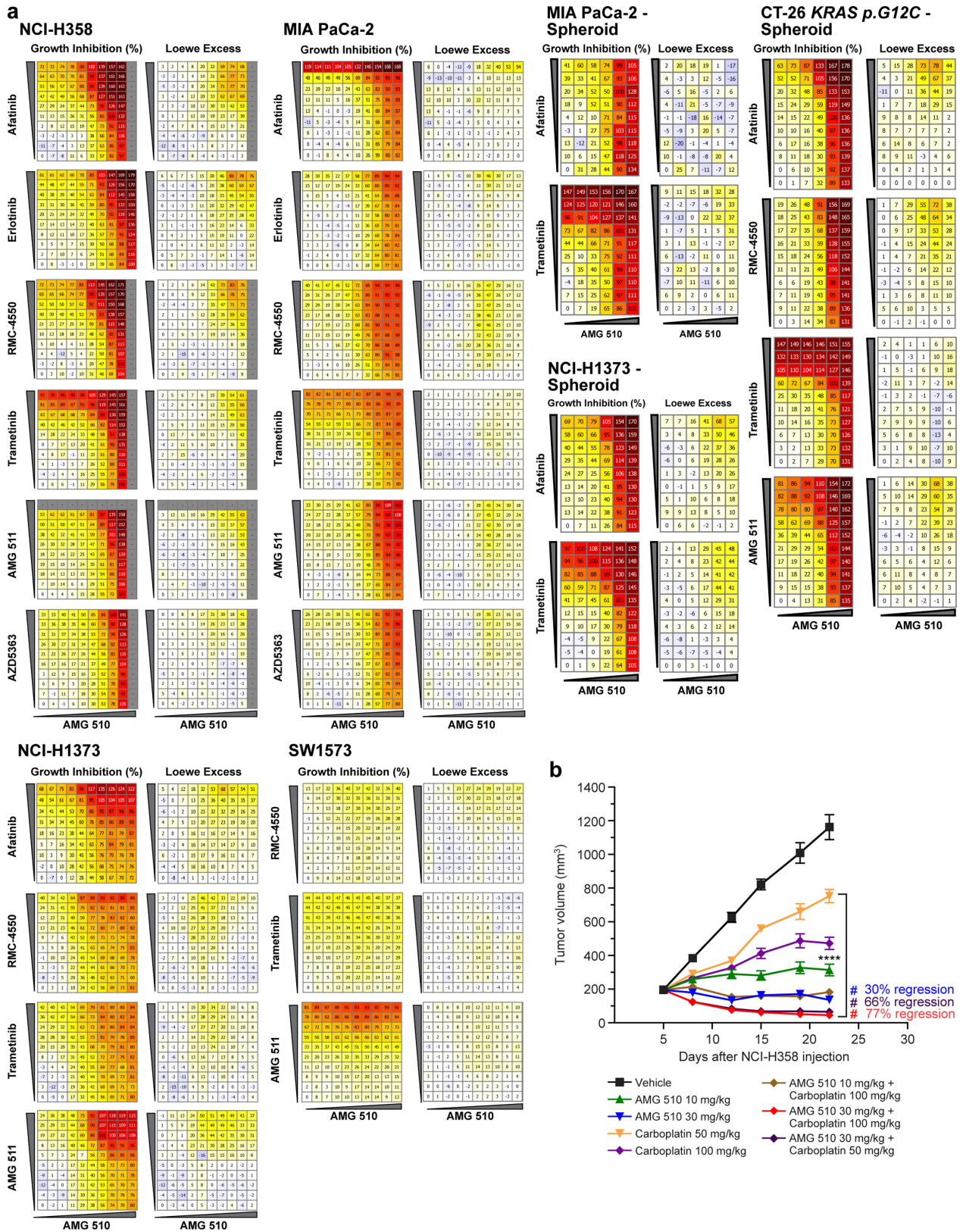
**Extended Data Fig. 4 | AMG 510 inhibits tumour growth of patient-derived xenografts, and exposure to AMG 510 at or above cellular IC<sub>90</sub> drives regression of xenografts.** **a**, Mice bearing MIA PaCa-2 T2 tumours were treated with ARS-1620 at the indicated doses. Data are mean  $\pm$  s.e.m.,  $n=10$  mice per group; \*\*\* $P<0.0001$ , \*\* $P<0.001$ , \* $P<0.05$  compared with vehicle; repeated-measures ANOVA followed by Dunnett's multiple-comparison test. # $P<0.05$  regression by two-sided Student's *t*-test. **b, c**, Plasma levels of AMG 510 from MIA PaCa-2 T2 or NCI-H358 xenografts. The dotted line represents the p-ERK IC<sub>90</sub> values in cells after treatment with AMG 510 for 2 h. **d, e**, Effect of AMG 510

treatment on tumour growth in *KRAS*<sup>G12C</sup> small-cell lung cancer (SCLC) and non-small-cell lung cancer (NSCLC) PDX models (**d**) or a SW480-1AC xenograft model (**e**). Data are mean  $\pm$  s.e.m.,  $n=10$  mice per group. \*\*\* $P<0.0001$  compared with vehicle; repeated-measures ANOVA followed by Dunnett's multiple-comparison test. **f**, Plasma levels of AMG 510 from CT-26 *KRAS*<sup>G12C</sup> tumour model. The dotted line represents the p-ERK IC<sub>90</sub> values in cells after treatment with AMG 510 for 2 h. **g**, Individual CT-26 *KRAS*<sup>G12C</sup> tumour plots of BALB/c nude mice ( $n=10$ ) treated with AMG 510 (200 mg kg<sup>-1</sup>).



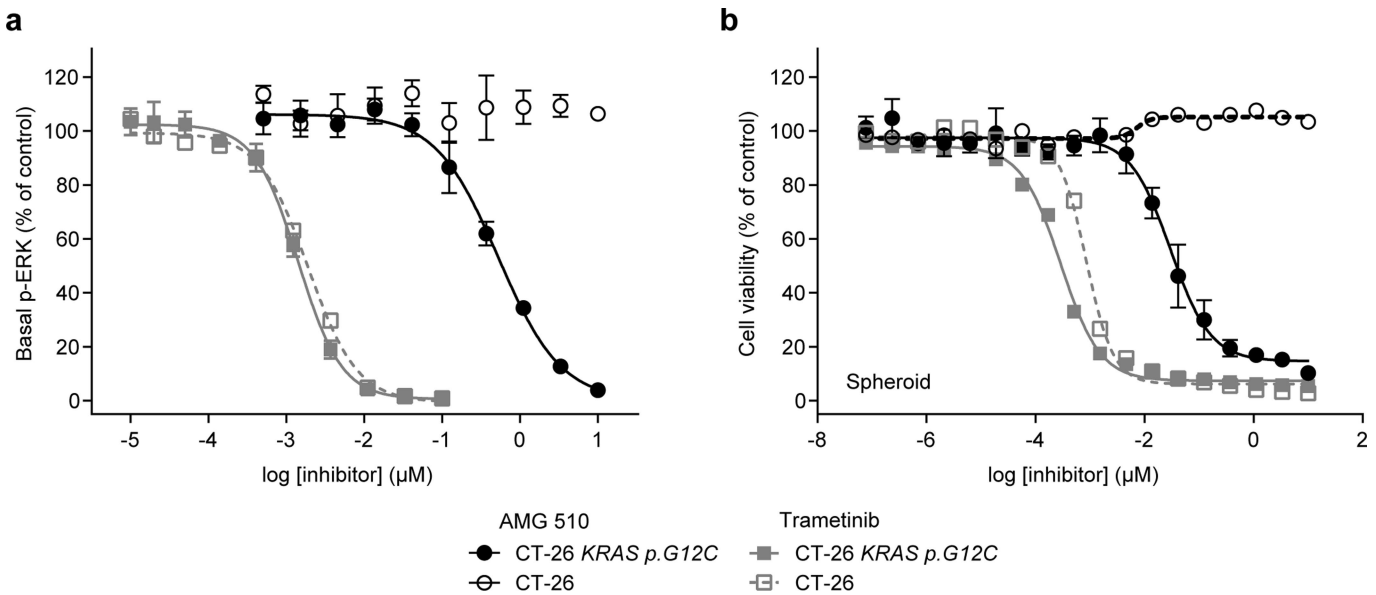
**Extended Data Fig. 5 | Clinical activity of AMG 510 in patients with lung cancer in a first-in-human dose-escalation study.** Computed tomography scans of two patients with *KRAS*<sup>G12C</sup> lung carcinoma who were treated with AMG 510. Additional representative pre-treatment (baseline) and post-treatment ( $R_x$ ) scans of patients described in Fig. 3 (left, 180 mg; right, 360 mg). Lesions are

denoted by red outline or red arrows. Left images show, from top to bottom, the lung upper left lobe, lung lower left lobe, lung upper left lobe and lung upper left lobe. Right images show, from top to bottom, the lung lower left lobe, lung lower left lobe and adrenal gland. Lesions in the 18-week scans of the patient who was treated with 360 mg AMG 510 were considered too small to accurately measure.



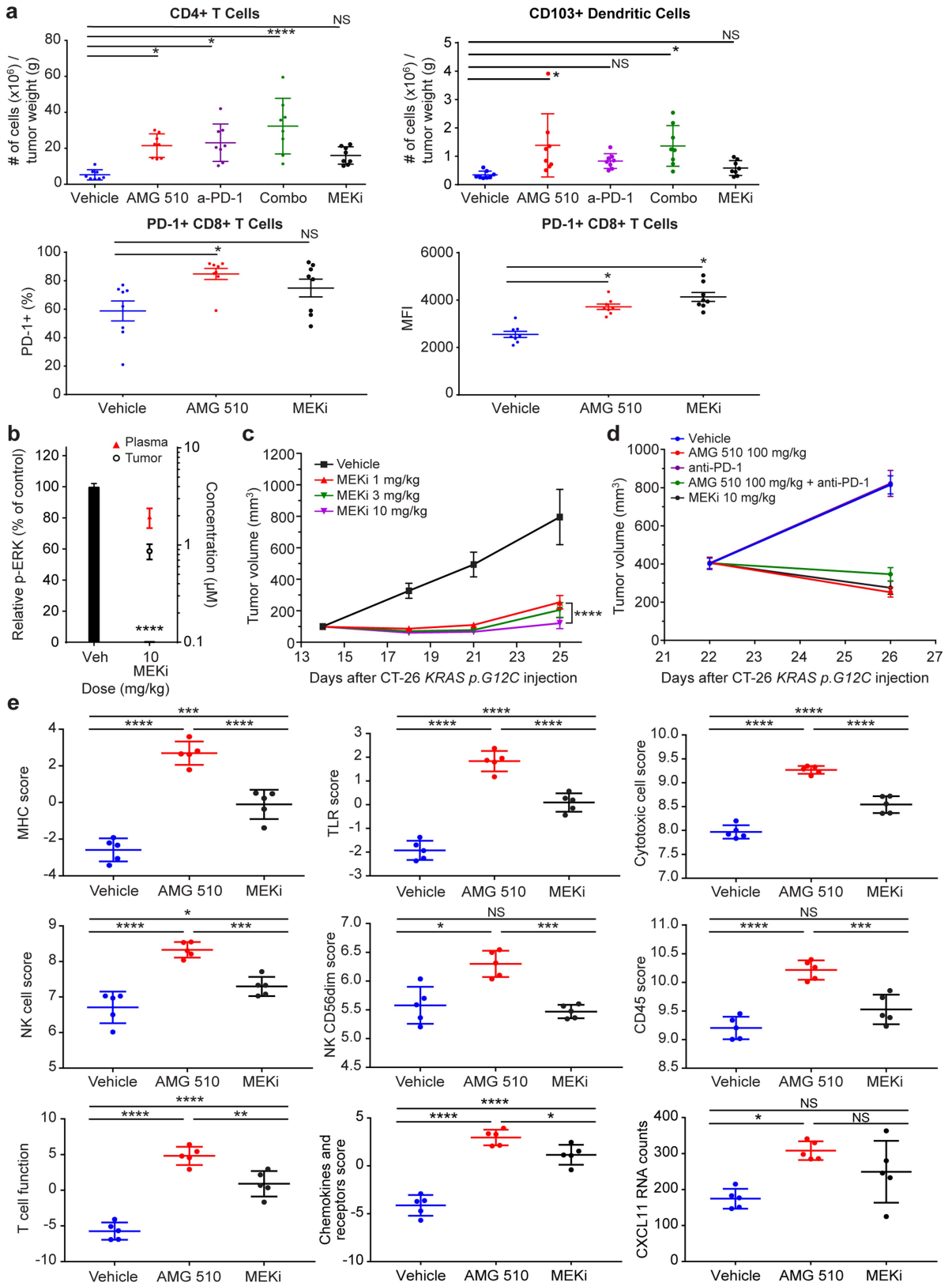
**Extended Data Fig. 6 | AMG 510 combines with targeted and chemotherapeutic agents, resulting in the synergistic killing of tumour cells and enhanced anti-tumour activity.** **a**, Growth inhibition matrices and Loewe additivity excess of AMG 510 added in combination with targeted agents to the indicated cell line, with darker colours denoting greater cell killing (growth inhibition) and stronger synergistic interactions (Loewe excess). The

maximum tested concentration of the inhibitors and the dose range covered by the matrices for each combination are listed in Supplementary Table 3. **b**, AMG 510 in combination with carboplatin in NCI-H358 tumour xenografts. Data are mean  $\pm$  s.e.m.,  $n=10$  mice per group; \*\*\* $P<0.0001$  compared with vehicle; repeated-measures ANOVA followed by Dunnett's multiple comparison test; # $P<0.001$  regression by two-sided Student's *t*-test.



**Extended Data Fig. 7 | AMG 510 inhibits KRAS(G12C) signalling and viability of syngeneic CT-26 KRAS<sup>G12C</sup> cells.** **a, b**, Cellular activity of AMG 510 and the MEK inhibitor trametinib in CT-26 KRAS<sup>G12C</sup> and parental CT-26 cell lines as measured by the inhibition of p-ERK after a 2-h treatment (**a**; mean  $\pm$  s.d.,  $n=3$  replicates;

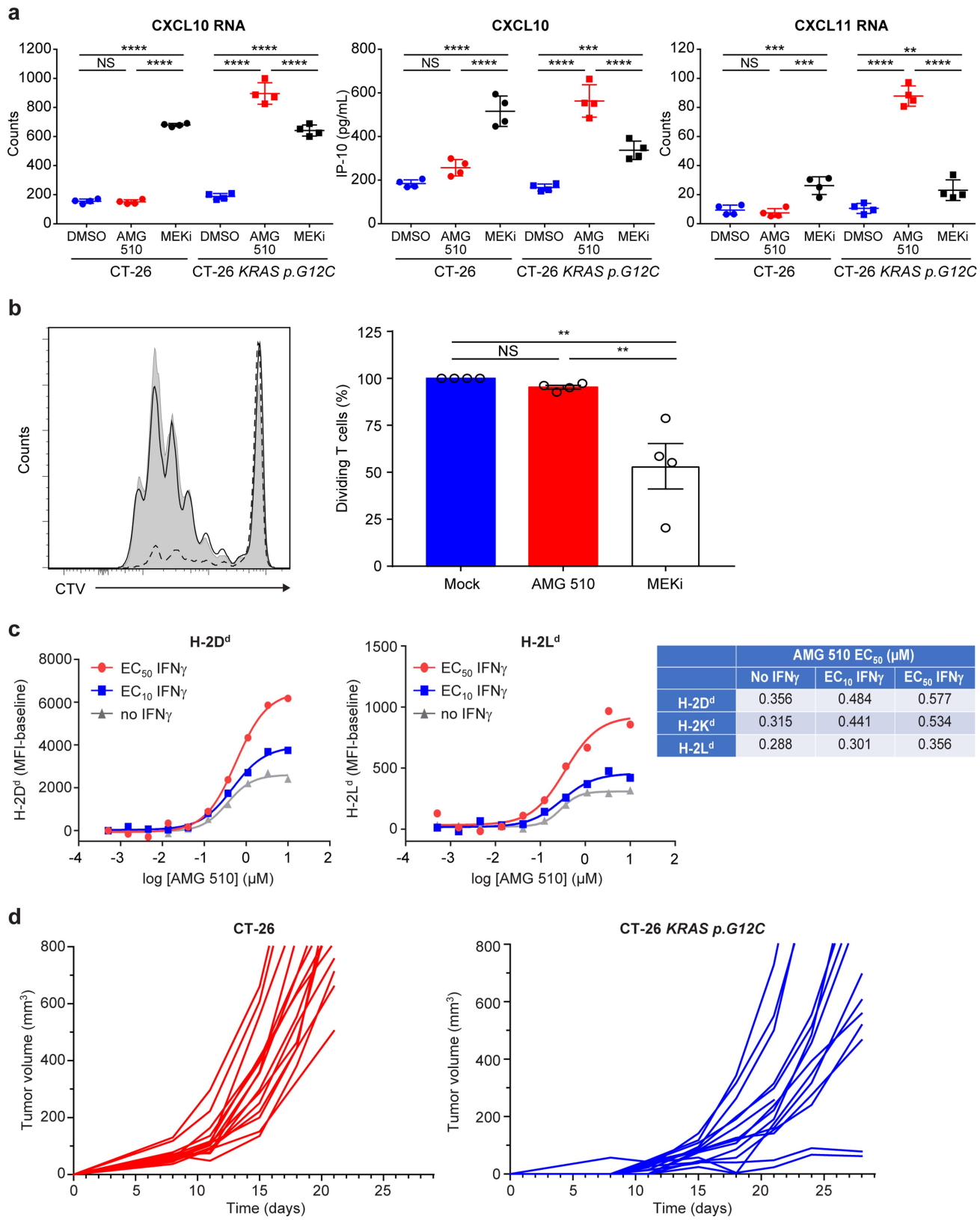
except trametinib in CT-26, mean of  $n=2$  replicates) and the effects on cell viability after 72-h treatment in spheroid culture (**b**; AMG 510 in CT-26 KRAS<sup>G12C</sup>, mean  $\pm$  s.d.,  $n=3$  replicates; all others, mean of  $n=2$  replicates).



**Extended Data Fig. 8** | See next page for caption.

## Article

**Extended Data Fig. 8 | AMG 510 treatment induces a pro-inflammatory tumour microenvironment.** **a**, CT-26 *KRAS*<sup>G12C</sup> tumours were immunophenotyped by flow cytometry. Data are mean  $\pm$  s.d.,  $n=8$  mice per group; \*\*\*\* $P<0.0001$ , \* $P<0.05$ ; NS, not significant; one-way ANOVA followed by Tukey's multiple-comparison test. MEKi, MEK inhibitor. **b**, Mice bearing CT-26 *KRAS*<sup>G12C</sup> tumours were treated orally with a single dose of vehicle (black bar) or with the indicated dose of MEK inhibitor (blue bar). Tumours were collected 2 h later and levels of p-ERK were measured. MEK inhibitor concentrations in plasma (red triangle) or tumours (black open circle). Data are mean  $\pm$  s.e.m.,  $n=3$  mice per group; \*\*\*\* $P<0.0001$  compared with vehicle; one-way ANOVA followed by Dunnett's multiple-comparison test. **c**, Mice bearing CT-26 *KRAS*<sup>G12C</sup> tumours were treated with MEK inhibitor at the indicated doses. Data are mean  $\pm$  s.e.m.,  $n=8$  mice per group; \*\*\*\* $P<0.0001$  compared with vehicle; repeated-measures ANOVA followed by Dunnett's multiple comparison test. **d**, Tumour volumes from the immunophenotyping study (**a**) of CT-26 *KRAS*<sup>G12C</sup> tumour-bearing mice treated over 4 days.  $n=8$  mice per group. **e**, RNA was isolated from CT-26 *KRAS*<sup>G12C</sup> tumours.  $n=5$  mice per group. Gene expression and scores were calculated by nSolver v.4.0. Data are mean  $\pm$  s.d.; \*\*\*\* $P<0.0001$ , \*\*\* $P<0.001$ , \*\* $P<0.01$ , \* $P<0.05$ ; NS, not significant; one-way ANOVA followed by Tukey's test.



**Extended Data Fig. 9** | See next page for caption.

# Article

**Extended Data Fig. 9 | AMG 510 induces expression of chemokines and MHC class I antigens in CT-26 *KRAS*<sup>G12C</sup> cells.** **a**, Quantification of *Cxcl10* or *Cxcl11* transcripts, as well as secreted CXCL10 (IP-10) protein, after 24-h treatment of parental CT-26 or CT-26 *KRAS*<sup>G12C</sup> cells with AMG 510 or MEK inhibitor. Data are mean  $\pm$  s.d.,  $n=4$  replicates; \*\*\*\* $P<0.0001$ , \*\*\* $P<0.001$ , \*\* $P<0.01$ ; NS, not significant; two-way ANOVA followed by Tukey's multiple-comparison test. **b**, Ova-pulsed bone-marrow-derived dendritic cells and CellTrace Violet (CTV)-labelled OT-ICD8<sup>+</sup> T cells co-cultured with AMG 510 or MEK inhibitor. T cell proliferation was assessed by measuring CTV dilution in T cells. Left, T cells

treated with mock (shaded), AMG 510 (solid line) or MEK inhibitor (dashed line) from a representative experiment. Right, data from four independent experiments were pooled and show the frequency of dividing T cells relative to mock treatment. Data are mean  $\pm$  s.e.m.; \*\* $P<0.01$ ; NS, not significant; one-way ANOVA followed by Tukey's multiple-comparison test. **c**, Cell surface expression of MHC class I antigens (H-2D<sup>d</sup> and H-2L<sup>d</sup>) on CT-26 *KRAS*<sup>G12C</sup> cells after 24-h treatment with AMG 510 with or without IFN $\gamma$  as measured by flow cytometry. **d**, Growth curves of either CT-26 or CT-26 *KRAS*<sup>G12C</sup> tumours in BALB/c mice ( $n=15$ ).

**Extended Data Table 1 | Data collection and refinement statistics for AMG 510-KRAS(G12C) complex**

KRAS <sup>G12C/C51S/C80L/C118S</sup> AMG 510 ( <b>6OIM</b> )	
<b>Data collection</b>	
Space group	P 21 21 21
Cell dimensions	
<i>a, b, c</i> (Å)	40.87, 58.42, 65.89
$\alpha, \beta, \gamma$ (°)	90, 90, 90
Resolution (Å)	30.0-1.65 (1.71-1.65)
$R_{\text{sym}}$	0.162 (0.521)
$I/\sigma I$	6.9 (2.5)
Completeness (%)	97.0 (96.3)
Redundancy	4.4 (4.2)
<b>Refinement</b>	
Resolution (Å)	30.00 - 1.65
No. reflections	18077
$R_{\text{work}} / R_{\text{free}}$	0.1809 / 0.2152
No. atoms	1613
Protein	1336
Ligand/ion	70
Water	207
$B$ -factors	24.8
Protein	24.3
Ligand/ion	24.1
Water	34.1
R.m.s. deviations	
Bond lengths (Å)	0.005
Bond angles (°)	1.08

One crystal dataset was collected for the X-ray co-crystal structure of the AMG 510-KRAS(G12C) covalent complex. Values in parentheses are for the highest-resolution shell.

# Reporting Summary

Nature Research wishes to improve the reproducibility of the work that we publish. This form provides structure for consistency and transparency in reporting. For further information on Nature Research policies, see [Authors & Referees](#) and the [Editorial Policy Checklist](#).

## Statistics

For all statistical analyses, confirm that the following items are present in the figure legend, table legend, main text, or Methods section.

n/a Confirmed

- The exact sample size ( $n$ ) for each experimental group/condition, given as a discrete number and unit of measurement
- A statement on whether measurements were taken from distinct samples or whether the same sample was measured repeatedly
- The statistical test(s) used AND whether they are one- or two-sided  
*Only common tests should be described solely by name; describe more complex techniques in the Methods section.*
- A description of all covariates tested
- A description of any assumptions or corrections, such as tests of normality and adjustment for multiple comparisons
- A full description of the statistical parameters including central tendency (e.g. means) or other basic estimates (e.g. regression coefficient) AND variation (e.g. standard deviation) or associated estimates of uncertainty (e.g. confidence intervals)
- For null hypothesis testing, the test statistic (e.g.  $F$ ,  $t$ ,  $r$ ) with confidence intervals, effect sizes, degrees of freedom and  $P$  value noted  
*Give P values as exact values whenever suitable.*
- For Bayesian analysis, information on the choice of priors and Markov chain Monte Carlo settings
- For hierarchical and complex designs, identification of the appropriate level for tests and full reporting of outcomes
- Estimates of effect sizes (e.g. Cohen's  $d$ , Pearson's  $r$ ), indicating how they were calculated

*Our web collection on [statistics for biologists](#) contains articles on many of the points above.*

## Software and code

Policy information about [availability of computer code](#)

### Data collection

B3 v3 (x-ray crystallography)  
EnVision Manager v1.13-1.14 (nucleotide exchange, viability, combination assays)  
Discovery Workbench v4.0 (p-ERK assays)  
ImageLab v4.1 and v5.2.1 (immunoblotting)  
Agilent RapidFire v4.0, MassHunter Workstation B.05.01 (mass spectrometry kinetic assay)  
nSolver v4.0 (NanoString)  
StudyDirector v3.1 (in vivo studies)  
BD FACSDiva v8.0.1(flow cytometry)  
Immunospot v2.6.1 (ELIspot)  
Analyst v1.6 (AMG 510-KRAS G12C conjugate detection, SILAC)

### Data analysis

CCP4 Program Suite v6.4.0, HKL2000 v717, MolRep v11.2.08, Refmac v5.8.0073, Coot v0.7.2, PRODRG v050106.0517 (x-ray crystallography)  
Microsoft Excel for Office 365 (nucleotide exchange, viability, p-ERK, kinetic, ELIspot, cysteine proteomics, flow cytometry)  
GraphPad Prism v7.04 (nucleotide exchange, viability, p-ERK, kinetic, in vivo efficacy/survival, flow cytometry, NanoString, ELIspot, SILAC)  
MassHunter Qualitative Analysis B.07.00 (mass spectrometry kinetic assay)  
Chalice Analyzer v1.5.0.71 (combination synergy scores)  
SEQUEST (cysteine proteomics)  
nSolver v4.0 (NanoString)  
Mathematica v11.3 (SILAC)  
Immunospot v2.6.1 (ELIspot)  
BD FACSDiva v8.0.1, FlowJo software v10 (flow cytometry)  
Biostatistical Analysis R Shiny application v1.0.5 (in vivo PKPD studies)

For manuscripts utilizing custom algorithms or software that are central to the research but not yet described in published literature, software must be made available to editors/reviewers. We strongly encourage code deposition in a community repository (e.g. GitHub). See the Nature Research [guidelines for submitting code & software](#) for further information.

## Data

Policy information about [availability of data](#)

All manuscripts must include a [data availability statement](#). This statement should provide the following information, where applicable:

- Accession codes, unique identifiers, or web links for publicly available datasets
- A list of figures that have associated raw data
- A description of any restrictions on data availability

The majority of data generated or analyzed during this study are included in this published article or available at the source data links. X-ray crystallographic coordinates and structure factor files have been deposited in the Protein Data Bank (PDB ID code: 6OIM). Other data that support the findings of this study are available from the corresponding authors. Qualified researchers may request data from Amgen clinical studies. Complete details are available here: <http://www.amgen.com/datasharing>.

## Field-specific reporting

Please select the one below that is the best fit for your research. If you are not sure, read the appropriate sections before making your selection.

Life sciences       Behavioural & social sciences       Ecological, evolutionary & environmental sciences

For a reference copy of the document with all sections, see [nature.com/documents/nr-reporting-summary-flat.pdf](http://nature.com/documents/nr-reporting-summary-flat.pdf)

## Life sciences study design

All studies must disclose on these points even when the disclosure is negative.

Sample size	For in vivo PKPD studies, n=3/group were used. For efficacy studies, n=8-10 mice per group were used. Animal numbers for in vivo studies were selected using power analysis alpha 0.05 and 80% power such that a minimum change of 32-49% could be detected on the observed data scale. No sample size calculation was performed for in vitro studies.
Data exclusions	No data were excluded.
Replication	In vitro experiments were repeated the indicated number of times, with the exception of immunoblot experiments which were performed once. Synergy scores were determined from the aggregate of two 10x10 matrices for adherent monolayer combinations, but only one 6x10 matrix for spheroid combinations. In vivo PKPD dose response studies (MIA PaCa-2 T2, CT-26 KRAS p.G12C) were repeated with similar results at least twice. The combination of AMG 510 with anti-PD-1 in CT-26 KRAS p.G12C, as well as the tumor growth measurements of untreated CT-26 parental and CT-26 KRAS p.G12C tumors, were repeated twice with similar results. All other in vivo studies were performed once. Independent repeats and sample sizes, as well as statistical analyses and significance levels, are also indicated in the Figure legends or in the Statistics and Reproducibility section.
Randomization	Sample randomization is not relevant to the in vitro studies presented. For in vivo studies, animals were evenly distributed such that each group had a similar mean and SEM at the start of the study.
Blinding	Treatment groups for the in vivo combination studies were blinded to the investigator.

## Reporting for specific materials, systems and methods

We require information from authors about some types of materials, experimental systems and methods used in many studies. Here, indicate whether each material, system or method listed is relevant to your study. If you are not sure if a list item applies to your research, read the appropriate section before selecting a response.

### Materials & experimental systems

n/a	Involved in the study
<input type="checkbox"/>	<input checked="" type="checkbox"/> Antibodies
<input type="checkbox"/>	<input checked="" type="checkbox"/> Eukaryotic cell lines
<input checked="" type="checkbox"/>	<input type="checkbox"/> Palaeontology
<input type="checkbox"/>	<input checked="" type="checkbox"/> Animals and other organisms
<input type="checkbox"/>	<input checked="" type="checkbox"/> Human research participants
<input type="checkbox"/>	<input checked="" type="checkbox"/> Clinical data

### Methods

n/a	Involved in the study
<input checked="" type="checkbox"/>	<input type="checkbox"/> ChIP-seq
<input type="checkbox"/>	<input checked="" type="checkbox"/> Flow cytometry
<input checked="" type="checkbox"/>	<input type="checkbox"/> MRI-based neuroimaging

## Antibodies

### Antibodies used

Immunoblot: all antibodies were used at 1:1,000 dilution unless otherwise indicated.  
phospho-EGF Receptor (Tyr1068) (D7A5) XP® Rabbit mAb Cell Signaling #3777; Lot 13

EGF Receptor (D38B1) XP® Rabbit mAb Cell Signaling #4267; Lot 11  
 Phospho-MEK1/2 (Ser217/221) Antibody Cell Signaling #9121; Lot 44  
 MEK1/2 Antibody Cell Signaling #9122; Lot 14  
 Phospho-S6 Ribosomal Protein (Ser235/236) (D57.2.2E) XP® Rabbit mAb Cell Signaling #4858; Lot 16  
 S6 Ribosomal Protein (5G10) Rabbit mAb Cell Signaling #2217; Lot 7  
 Phospho-Akt (Ser473) (D9E) XP® Rabbit mAb Cell Signaling #4060; Lot 19  
 Akt Antibody Cell Signaling #9272, Lot 27  
 Phospho-ERK1/ERK2 (Thr185, Tyr187) Polyclonal Antibody ThermoFisher #44-680G; Lot SB248818  
 p44/42 MAPK (Erk1/2) Antibody Cell Signaling #9102; Lot 26  
 Anti-Ras antibody [EPR3255] Abcam #ab108602; Lot GR117071-23  
 Cleaved Caspase-3 (Asp175) Antibody Cell Signaling #9661; Lot 45  
 Anti-β-Actin-Peroxidase Mouse mAb AC-15 Sigma #A3854; Lot 026M4820V; 1:20,000  
 Donkey Anti-rabbit IgG HRP GE Healthcare #NA934V; Lot 9677977; 1:5,000

Flow cytometry: all antibodies were used at 1:100 unless otherwise indicated.  
 PE Mouse anti-mouse H-2Dd (34-2-12, Biolegend #110608, Lot B256526)  
 PE Mouse anti-mouse H-2Kd (SF1-1.1, Biolegend #116608, Lot B244820)  
 PE Mouse anti-mouse H-2Ld/H-2Db (28-14-8, Biolegend #114507, Lot B240332)  
 BUV737 rat anti-mouse CD4 (RM4-5, BD Biosciences #564933, Lot 8164630)  
 BV421 rat anti-mouse CD8a (53-6.7, BD Biosciences #563898, Lot 7201962)  
 BUV737 rat anti-CD11b (M1/70, BD Biosciences #564443, Lot 7338572)  
 BV786 mouse anti-mouse CD45.2 (104, BD Biosciences #563686, Lot 8235903)  
 APC-H7 rat anti-mouse Ly-6G (1A8, BD Biosciences #565369, Lot 8121728)  
 BV711 hamster anti-mouse TCR B chain (H57-597, BD Biosciences #563135, Lot 7054698)  
 FITC rat anti-mouse CD24 (M1/69, ThermoFisher #11-0242-81, Lot 1937898)  
 APC hamster anti-mouse CD103 (2E7, ThermoFisher #17-1031-80, Lot 17-1031-80)  
 PE hamster anti-mouse CD279 (PD-1) (J43, ThermoFisher#12-9985-82, Lot 4329622)  
 APC/Cy7 rat anti-mouse CD90.2 (30-H12, Biolegend #105328, Lot B241601)  
 BV650 rat anti-mouse F4/80 (BM8, Biolegend #123149, Lot B256505)  
 BV711 rat anti-mouse Ly-6C (HK1.4, Biolegend #128037, Lot B247973)  
 BV510 rat anti-mouse I-A/I-E (MHCI) (M5/114.15.2, Biolegend #107635, Lot B263357)  
 APC rat anti-mouse CD8a (53-6.7, eBioscience #17-0081-82, Lot E07056-1635)  
 rat anti-mouse CD16/CD32 (2.4G2, BD Biosciences #553142, Lot 4198965)  
 FITC hamster anti-mouse TCR B chain (H57-597, BD Biosciences #553171, Lot 8351664)

#### Immunohistochemistry:

Rat anti-human CD3 (mouse CD3 cross-reactive) (CD3-12, Bio-Rad #MCA1477, Lot 7708); 1:1,000  
 Rabbit anti-mouse CD8a (D4W2Z, Cell Signaling Technology #98941, Lot 0712017); 1:500  
 Rabbit anti-human Ki67 (mouse Ki67 cross-reactive) (SP6, Sigma-Aldrich #275R-1, Lot 45305); 1:500  
 Rat IgG isotype negative control (Jackson ImmunoResearch Labs #012-000-003, Lot 68714); 2 mcg/mL  
 Rabbit IgG isotype negative control (Jackson ImmunoResearch Labs #011-000-003, Lot 132409); 2 mcg/mL  
 HRP-anti-rat-IgG (Biocare Medical #BRR4016L, Lot 100317); undiluted  
 HRP-anti-rabbit-IgG (Dako #K4003, Lot 10147964); undiluted

#### Validation

All antibodies were validated by the manufacturer. Please refer to the manufacturers' websites with the catalog information listed above.

## Eukaryotic cell lines

#### Policy information about [cell lines](#)

##### Cell line source(s)

The following cell lines were purchased from American Type Culture Collection (ATCC): MIA PaCa-2, NCI-H1373, NCI-H2030, NCI-H2122, SW1463, SW1573, UM-UC-3, Calu-1, NCI-H1792, NCI-H23, NCI-H358, SW837, AsPC-1, A-427, LS 174T, SW480, A549, NCI-H1355, HCC-827, COLO-205. KM12 and NCI-H3122 were obtained from the Amgen internal cell bank, originally sourced from the National Cancer Institute.

MIA PaCa-2 T2 and SW480-1AC cells were generated by passaging MIA PaCa-2 and SW480 cells, respectively, in mice.

CT-26 KRAS p.G12C cells were generated from the murine CT-26 colorectal line (ATCC) using CRISPR technology to replace both KRAS p.G12D alleles with p.G12C (ThermoFisher Scientific).

##### Authentication

Cell lines were authenticated by short tandem repeat (STR) profiling or were used immediately after purchase from ATCC.

##### Mycoplasma contamination

All cell lines used for in vivo studies were confirmed to be negative for mycoplasma contamination.

##### Commonly misidentified lines (See [ICLAC](#) register)

No commonly misidentified cell lines were used.

## Animals and other organisms

#### Policy information about [studies involving animals; ARRIVE guidelines](#) recommended for reporting animal research

##### Laboratory animals

BALB/c or athymic nude mice, all female, all 6-12 weeks of age.

Wild animals

Studies did not involve wild animals.

Field-collected samples

Studies did not involve samples collected in the field.

Ethics oversight

All animal experimental protocols were approved by the Amgen Animal Care and Use Committee and were conducted in accordance with the guidelines set by the Association for Assessment and Accreditation of Laboratory Animal Care.

Note that full information on the approval of the study protocol must also be provided in the manuscript.

## Human research participants

Policy information about [studies involving human research participants](#)

Population characteristics

See clinicaltrials.gov NCT03600883.

Key inclusion criteria: age  $\geq 18$ ; documented locally-advanced or metastatic KRASG12C; measurable or evaluable disease; ECOG  $\leq 2$ ; life expectancy  $>3$  months (mo). Key exclusion criteria: active brain metastases; myocardial infarction within 6 mo.

Recruitment

Patients were recruited at clinical study sites based on the presence of the KRAS p.G12C mutation in their tumor by standard genotype testing.

Ethics oversight

Clinical trial NCT03600883 was conducted in compliance with all relevant ethical regulations. The protocol was approved by the institutional review boards (IRB)/independent ethics committees (IEC) of all clinical study sites.

Note that full information on the approval of the study protocol must also be provided in the manuscript.

## Clinical data

Policy information about [clinical studies](#)All manuscripts should comply with the ICMJE [guidelines for publication of clinical research](#) and a completed [CONSORT checklist](#) must be included with all submissions.

Clinical trial registration

NCT03600883

Study protocol

Study is ongoing; clinical trial information is available on clinicaltrials.gov

Data collection

This multicenter, open-label, 1st in human, phase 1 study (NCT03600883) evaluates safety, tolerability, PK/pharmacodynamics (PK/PD), and efficacy of AMG 510 in patients (pts) with KRASG12C advanced solid tumors. Primary endpoint: safety [eg, adverse events (AEs); dose limiting toxicities (DLT)]; key secondary endpoints: PK, ORR (overall response rate)[assessed every 6 weeks (wks)] and PFS (progression free survival). Key inclusion criteria: age  $\geq 18$ ; documented locally-advanced or metastatic KRASG12C; measurable or evaluable disease; ECOG  $\leq 2$ ; life expectancy  $>3$  months (mo). Key exclusion criteria: active brain metastases; myocardial infarction within 6 mo. Sequential dose escalation cohorts are enrolled to evaluate safety, tolerability, PK/PD and to find the maximum tolerated dose (MTD). After identifying the MTD, 60 pts with advanced KRASG12C STs can enroll. Daily oral AMG 510 is given until disease progression (PD), intolerance, or consent withdrawal.

Clinical data presented in this manuscript was collected at participating clinical sites from September 2018 through June 2019.

Outcomes

The endpoints described in this manuscript were based on RECIST 1.1 criteria for clinical responses.

## Flow Cytometry

### Plots

Confirm that:

- The axis labels state the marker and fluorochrome used (e.g. CD4-FITC).
- The axis scales are clearly visible. Include numbers along axes only for bottom left plot of group (a 'group' is an analysis of identical markers).
- All plots are contour plots with outliers or pseudocolor plots.
- A numerical value for number of cells or percentage (with statistics) is provided.

### Methodology

Sample preparation

For in vitro studies, cells were non-enzymatically detached from the wells, washed with staining buffer (PBS/0.5% BSA), and then incubated with PE-conjugated H-2Dd, H-2Kd, or H-2Ld antibodies (BioLegend) for 30 minutes on ice. After washing, cells were resuspended in staining buffer containing SYTOX Blue Dead Cell Stain (Life Technologies), and then analyzed by flow cytometry.

For co-cultures, CellTrace Violet-labeled CD8+ T cells from spleens of OT-I transgenic mice were combined with bone marrow-derived dendritic cells (BMDCs) in 96-well plates with or without further AMG 510 or MEKi treatment. Co-cultures were incubated for three days at 37°C. Cell division was assessed by flow cytometry by measuring CTV dilution in TCR $\beta$ + CD8 $\alpha$ + cells.

For in vivo studies, tumors were harvested, weighed, minced, and placed in Liberase TL (0.2 mg/ml; Roche) and DNase I (20  $\mu$ g/ml; Ambion). Tumor cell suspensions were then homogenized using a gentle MACS Dissociator (Miltenyi Biotech) and incubated

at 37°C for 15 minutes on a MACSmix Tube Rotator (Miltenyi Biotech). Cells were then treated with 0.02% EDTA (Sigma) and heat-inactivated FBS (ThermoFisher Scientific) and filtered to remove clumps. After centrifugation, the cell pellets were resuspended in LIVE/DEAD Fixable Blue Dead Cell Stain (ThermoFisher Scientific) for 30 minutes. Cell surface staining was performed with the indicated antibodies (see Antibodies section above) before fixation and permeabilization of the cells (Intracellular Fixation & Permeabilization Buffer Set, eBiosciences) for intracellular staining. CountBright™ Absolute Counting Beads (ThermoFisher Scientific) were added to each sample before analysis on an LSR II flow cytometer (BD Biosciences). All analyses were performed with FlowJo software v10 (FlowJo). Absolute cell counts were determined by normalizing cell numbers to beads recorded, divided by the volume of tumor aliquot analyzed and the mass of the tumor.

**Instrument**

In vitro samples were run on a BD LSRFortessa. In vivo samples were run on a LSR II flow cytometer (BD Biosciences).

**Software**

All analyses were performed with either BD FACSDiva or FlowJo software v10.

**Cell population abundance**

*Describe the abundance of the relevant cell populations within post-sort fractions, providing details on the purity of the samples and how it was determined.*

**Gating strategy**

For in vitro experiments, FSC-H/FSC-A gate was used to identify single cells and eliminate doublets from the analysis. FSC/SSC gate (P1) was used to gate on the population of CT-26 KRAS p.G12C cells. Cells from P1 were displayed on a histogram and SYTOX Blue negative cells were gated on to identify live cells. The mean fluorescent intensity (MFI) of MHC class I antigen expression was measured on these live cells.

For co-culture experiments, lymphocytes were first gated using FSC/SSC. Live cells were then gated using 7AAD viability dye, followed by exclusion of doublets using SSC-A/SSC-H. CD8+ T cells were then gated using fluorescently labeled antibodies. Finally, CellTrace Violet dye incorporation was assessed on the CD8+ T cells.

For in vivo experiments, cells were gated first in intact cells using FSC/SSC. Cells were then gated on live cells using the viability dye, followed by cell type-specific gating using fluorescently labeled antibodies.

Tick this box to confirm that a figure exemplifying the gating strategy is provided in the Supplementary Information.